IMPA1 dependent regulation of plasma membrane phosphatidylinositol 4,5-bisphosphate turnover and calcium signalling by lithium

Sankhanil Saha, Harini Krishnan and Padinjat Raghu*
National Centre for Biological Sciences-TIFR
GKVK Campus, Bellary Road, Bangalore 560065, India

*corresponding author
E-mail: praghu@ncbs.res.in

Running Title- Lithium regulates PIP_2 and calcium signaling in human neurons

Abstract

Lithium (Li) is a widely used as a mood stabilizer in the clinical management of Bipolar Affective Disorder (BPAD). However, the molecular targets of Li in neural cells that underpin its therapeutic effect remain unresolved. Inositol monophosphatase (IMPA1), is an enzyme involved in the resynthesis of phosphatidylinositol 4,5-bisphosphate (PIP_2) following receptor-activated phospholipase C (PLC) signalling. *In vitro*, Li inhibits IMPA1, but the relevance of this inhibition within neural cells remains unknown. Here we report that in human cells, treatment with therapeutically relevant concentrations of Li reduces receptor activated calcium release from intracellular stores and also delays the resynthesis of PIP_2 following receptor activated PLC signalling. Both these effects of Li are abrogated in cells where IMPA1 has been deleted. We also observed that in human forebrain cortical neurons, treatment with Li results in reduced neuronal excitability as well as reduced calcium signals following receptor activated PLC signalling. Following Li treatment of human forebrain cortical neurons, transcriptome analyses reveal downregulation of multiple components of the glutamate receptor signalling system. Glutamate is a key excitatory neurotransmitter in the human brain and thus our findings provide an insight into the mechanisms underlying the dampening of neuronal excitability following Li treatment. Collectively, our findings suggest that Li inhibits receptor activated PLC signalling leading to an altered transcriptional response and reduced neuronal excitability.

Introduction

Bipolar affective disorder (BPAD) is a human psychiatric illness characterized by disruptive mood swings; the defining characteristics being the alteration between mania and depression [1] associated with an elevated rate of suicide among patients [2]. BPAD has been regarded by the World Health Organization (WHO) as one of the leading causes of disability worldwide [3]. Mood stabilizers like lithium (Li), Carbamazepine and Valproate remain the first-line mode of medication for bipolar disorder. Among these drugs, Li stands out as the go-to drug for treating acute manic phases and also for its preventive effect against relapses of manic episodes [4, 5]. Although Li remains the mainstay in BPAD treatment, individual patient responses towards Li arevariable- it remains ineffective for a large proportion (approximately 30%) of BPAD patients, the so-called 'Li non-responders', whereas another 30% of patients are only partially responsive to Li [6]. The reason for this variable response is unknown and remains a topic of intense interest.

Li responsiveness is determined clinically by functional improvement in brain function as determined using the Alda score following treatment [7]. Despite substantial research over several decades, the molecular and biochemical mechanism by which Li exerts its effects on human brain cells that are relevant to functional improvements remains unclear [8]. A large number of molecular targets for Li have been described [9]. These include Inositol monophosphatase (IMPase) [10], Glycogen synthasekinase-3β (GSK-3β) [11], Sodium myo-inositol co-transporter (SMIT1) [12] and Bisphosphate- 3'-nucleotidase (BPNT1) [13]. The two most well studied targets of Li are Inositol monophosphatase (IMPase) and Glycogen synthase kinase-3β (GSK-3β).

A long-standing hypothesis for the therapeutic effect of Li is its impact on inositol lipid turnover during receptor activated G-protein coupled signalling through inhibition of IMPase [10]. During GPCR signalling, many receptors activate Phospholipase C (PLC) leading to the hydrolysis of the signalling lipid Phosphatidylinositol 4,5-bisphosphate (PIP_2) generating inositol 1,4,5-trisphosphate (IP_3) and diacylglycerol (DAG) [11] ultimately leading to changes in intracellular calcium $[Ca^{2+}]_I$. Alterations in $[Ca^{2+}]_I$ have previously been reported in cell lines derived from BPAD patients [12]. PIP_2 is a low abundance membrane lipid and its resynthesis is required to sustain PLC signalling during high rates of PLC activity as is seen in the brain [13] during the activation of many GPCR required for neurotransmission such as the metabotropic glutamate receptor [14]. The resynthesis of PIP_2 occurs via a set of biochemical reactions referred to as the PIP_2 cycle [15]. The sequential dephosphorylation of IP_3 produced during PLC activity to generate inositol, is required for PIP_2 resynthesis (Fig

1A). IMPase is the enzyme required for the final step in the conversion of inositol 1-phosphate to inositol. Biochemical analyses showed a decrease in myo-inositol concentration in cerebral cortex of lithium-treated rats accompanied by an increase in the concentration of inositol monophosphate suggesting that Li might inhibit IMPase [16, 17]. Subsequent studies showed that Li binds to IMPase and inhibits the enzyme in a non-competitive manner [18]. These observations led Berridge to propose the “Inositol depletion hypothesis” [19] which posits that during PLC signalling in the brain, the inhibition of IMPase by Li restricts the supply of inositol for PIP_2 resynthesis leading to down regulation of neurotransmitter receptor signalling, thus reducing excitability in the brain and the control of mania.

The mammalian genome includes two genes encoding IMPase activity, IMPA1 and IMPA2. However, IMPA1 is more abundant in the human brain [20, 21] and is inhibited by Li at therapeutically relevant concentrations [22]. *In vivo* studies have also suggested a role of Li in regulating IMPase function. Briefly, (i) in rodent models, Li treatment reduced brain inositol levels and elevated Inositol monophosphate (IP_1), the substrate of IMPase in the cerebral cortex of rat [23] (ii) treatment of human BPAD patients with Li led to a reduction in PIP_2 levels in platelet membranes [24–26]. However, there are also findings that do not support this hypotheses (i) IMPA1 knockout mice showed only a modest reduction in brain inositol levels [27] and the impact of IMPA1 knockout on receptor activated PIP_2 turnover remains unknown, (ii) genome-wide association studies have not revealed polymorphisms in IMPA1 that are linked to BPAD or Li sensitivity [28][6].

In this study, we have tested the hypothesis that treatment of human cells with Li diminishes calcium signalling. We find that this change is underpinned by reductions in G-protein coupled PIP_2 turnover. These changes in calcium signalling were also observed in human iPSC derived forebrain cortical neurons and accompanied by reduction in neuronal excitability. Transcriptomic analysis revealed that Li treatment exerts its effect on neuronal excitability through multiple mechanisms including but not restricted to GPCR activated calcium signalling. Our findings open new approaches to predict Li responsiveness in BPAD patients and develop novel strategies for the clinical management of this disorder.

Materials and Methods

DNA constructs: For PIP_2 measurement, PH-PLCδ::GFP probe was used which was a gift from Tamas Balla (Addgene plasmid # 51407). The cDNA for human muscarinic acetylcholine receptor m1AchR was obtained from cDNA Resource Center (MAR0100000) and was cloned via Gibson assembly into a lentiviral pHR transfer backbone (having Puromycin resistance cassette) for lentiviral generation. The Nir2 shRNA was obtained from GE Dharmacon (RHS4430-200186441: Clone id V2LHS_62836).

Mammalian cell culture, treatment and transfection: HEK293T cells were maintained under standard conditions at (37°C, with 5% CO_2) in DMEM high Glucose media (Dulbecco's Modified Eagle Medium; Life Technologies), supplemented with 10% Foetal bovine serum. For Li treatment, the cells were grown and maintained in this media, supplemented with 1 mM LiCl (Sigma) for 5 days.The cells were tested for mycoplasma, prior to the experiments. MycoAlert™ (Lonza) was used per the manufacturer's protocol to test the spent media for mycoplasma contamination. Transfection with the plasmid expressing PH-PLCδ::GFP probe was done 24 hours before the imaging experiments using Polyethylenimine solution (PEI; Polysciences Inc.; 1 mg/ml) when the cells were around 70% confluent.

Lentiviral transduction to generate HEK293T cell line stably expressing muscarinic acetylcholine receptor m1AchR: Recombinant Lentiviral particles were packaged in HEK293T cells grown in DMEM high Glucose media, supplemented with 10% FBS. The HEK293T cells cultured in the 6 well plates were transfected with a solution consisting of 1.2 µg of pHR-IRES plasmid encoding muscarinic acetylcholine receptor *CHRM1* cDNA, along with 1.2 µg of each of the helper plasmids (psPAX and pMD2.G) in 500 µl of Opti-MEM (Invitrogen) and 110 µl Polyethylenimine (PEI, 1 mg/ ml). Medium was changed after 12 hours and the virus was harvested at 72 h after transfection. Then HEK293T cells were transduced with these recombinant viral particles and selected via Puromycin treatment (1.5 µg/ ml) for 1 week- to obtain the HEK293T cell line, expressing m1AchR. Western Blot confirming the expression of m1AchR is shown in supplementary figures (Supp. Fig 3C,D).

Generation of Neural Stem Cells and differentiation and maintenance of neuronal culture: Neural Stem Cells (NSCs) were generated as previously described [61], with slight modifications. Human iPSCs were differentiated to embryoid bodies in E6 medium (Gibco). After that, primary neural rosettes that were formed, were manually picked, passaged and eventually plated as NSC monolayer in Neural Expansion Medium (NEM; DMEM/F12 with 2mM Glutamax, supplemented with N2, B27 without Vitamin A, 20 ng/ml bFGF, 100 µM non-

181 essential amino acids, 2 µg/ml Heparin Sulphate, 100 U/ml penicillin-streptomycin) (all
182 components procured from Life Technologies). The NSCs were subjected to CD133+
183 selection as previously described via fluorescence-activated cell sorting (FACS) [62] to
184 eliminate cells of other lineages. The sorted NSCs were further characterized by
185 immunofluorescence for the specific markers. Neural Stem Cells (NSCs) were grown on
186 Matrigel coated tissue dishes in NEM at 37°C and 5% CO_2.
187
188 For differentiation, NSCs were seeded onto Matrigel- Growth Factor Reduced (Corning)
189 coated cover-slip dishes or 35 mm dishes and expanded in NEM till the cells reached 70%
190 confluency. NEM was then withdrawn and replaced with Neural Differentiation Medium
191 (NDM; DMEM/F12 with 2mM Glutamax, supplemented with N2, B27 containing Vitamin A,
192 100 µM non-essential amino acids, 100 U/ml penicillin-streptomycin, 10 ng/ml BDNF, 10
193 ng/ml GDNF, 10 ng/ml IGF-1, 50 µg/ml Ascorbic acid (Sigma) and 2 µM DAPT (Sigma)).
194 DAPT was supplemented for the first 14 days. Media was changed every 2 days during the
195 differentiation process. All the experiments were done 45 DIV post differentiation (The day of
196 addition of NDM was considered to be DIV 0). For chronic Li treatment, the neuronal cultures
197 were maintained in NDM supplemented with 1 mM LiCl for the last 10 days (DIV35 to
198 DIV45).
199
200 **Live cell imaging for the PIP_2 probe:** To analyse the dynamics of PIP_2 at the plasma
201 membrane by following the change in translocation of the PH-PLCδ::GFP probe, live cell
202 imaging was performed as stated in *Varnai et al* [31], with minor modifications. 20000 cells
203 were seeded in Poly-L Ornithine (PLO) coated cover-slip dishes and grown for 96 hours with
204 or without Li. 24 hours prior to imaging, the cells were transfected with PH-PLCδ::GFP
205 plasmid using Lipofectamine 3000 as per manufacturer's protocols. Carbamoylcholine
206 chloride mediated changes in the membrane localization of PH-PLCδ::GFP probe was
207 examined by a time-lapse method using an Olympus FV 3000 confocal microscope. The
208 cells were kept in pre-warmed Kreb's Ringer Buffer (120 mM NaCl, 4.7mM KCl, 1.2 mM
209 $CaCl_2$, 0.7 mM $MgSO_4$, 10 mM Glucose, 10 mM HEPES; pH-7.4) and at 37°C while imaging.
210 Changes in the PIP_2 membrane localization were quantified by taking a fluorescence
211 intensity ratio of the plasma membrane (F_{PM}) and the cytosol (F_{Cyt}) across the time-lapse and
212 normalizing it to the first value.
213
214 **Calcium Imaging for Carbamoylcholine stimulation:** For studying the calcium physiology,
215 HEK293T-M1 cells were seeded in Poly-L Ornithine (PLO) coated cover-slip dishes while
216 iPSC derived cortical neurons (DIV45) were grown on Matrigel coated cover-slip dishes.

217 Before imaging, the cells were washed twice with Hank's Buffered Salt Solution (HBSS) (10
218 mM HEPES, 118 mM NaCl, 4.96 mM KCl, 1.18 mM $MgSO_4$, 1.18 mM KH_2PO_4, 10 mM
219 Glucose, 2 mM $CaCl_2$; pH-7.4) and then loaded with the ratiometric Ca^{2+} indicator Fura-2 AM
220 (4 μM) (Acetoxymethylester, Invitrogen) along with 0.002% Pluronic F-127 for 30 minutes.
221 The excess dye was removed by washing the cells thrice with HBSS and cells were
222 incubated for an additional 20 minutes to equilibrate the intracellular dye concentration and
223 allow de-esterification. Imaging was performed for 10 min using a 40X objective (N.A. 0.75)
224 of wide-field fluorescence microscope Olympus IX-83 for HEK293T cells, while a 20X
225 objective (N.A. 0.50) was used for neuronal cultures. Free- and Ca^{2+}-bound Fura-2
226 fluorescence intensities (excitation 340/380 nm, emission 510 nm) were recorded at every 5
227 seconds intervals using an EM-CCD camera (Evolve 512 Delta, Photometrics). Basal
228 cytosolic Ca^{2+} was recorded in HBSS buffer for the initial 18 frames. Carbamoylcholine
229 chloride (20 μM and 50 μM respectively for HEK and neuronal cultures, as determined in
230 preliminary concentration–response experiments) (Sigma Aldrich-C4382) was added to the
231 cells for activating PLC and thereby, inducing Ca^{2+} release from the endoplasmic reticulum
232 store. After recording for 42 frames, 20 μM Ionomycin (Calbiochem) was added and
233 recorded for 24 frames for recording R_{max}. 24 more frames were recorded, post addition of 4
234 mM EGTA (containing 0.01% Triton-X-100) for chelation of Ca^{2+} ions and determination of
235 R_{min}.
236
237 **Calcium Imaging for SOCE (Store Operated Calcium Entry):** For the SOCE experiment,
238 the cells were kept in 'zero Ca^{2+} HBSS' (10 mM HEPES, 118 mM NaCl, 4.96 mM KCl, 1.18
239 mM $MgSO_4$, 1.18 mM KH_2PO_4, 10 mM Glucose; pH-7.4) just before the imaging. After
240 recording the initial 12 frames for basal cytosolic Ca^{2+}, an optimal concentration of
241 Thapsigargin (10 μM) (Invitrogen) was added for the store depletion and 60 frames were
242 recorded. Then, 2 mM $CaCl_2$ was then added to the extracellular buffer to induce SOCE- 60
243 frames were recorded post induction of SOCE. Subsequently, 20 μM Ionomycin
244 (Calbiochem) was added and recorded for 24 frames; then 4 mM EGTA (containing 0.01%
245 Triton-X-100) was added and 24 frames were recorded. For studying PLC activated calcium
246 mobilization from stores and SOCE, Carbamoylcholine chloride (20 μM and 50 μM
247 respectively for HEK and neuronal cultures) was added instead of Thapsigargin.
248
249 **Analysis of Calcium recordings:** The CellSens Olympus software was used for the
250 analysis. A dynamic region of interest (ROI) was drawn for each cell which exhibited rise in
251 $[Ca^{2+}]_I$ (as seen by increase in fluorescence post-stimulation) to track the fluorescence
252 changes over time. The emission intensities corresponding to 340 nm and 380 nm

253 excitations were used to calculate the 340/380 ratio for each cell across all time points. The
254 $[Ca^{2+}]_I$ was estimated using the Grynkiewicz equation [63] as follows:
255 $[Ca^{2+}]_I$ (nM) = K_d X SF X (R - R_{min})/ (R_{max}- R)
256 where R_{min} and R_{max} refer to the minimum and maximum 340/380 ratio respectively. 224 nM
257 was taken as K_d for Fura-2 AM in human cells and SF (scaling factor) was calculated for
258 each cell by dividing the fluorescence emission intensity at Ca^{2+} free form with the
259 fluorescence emission intensity at Ca^{2+} bound form of the dye after excitation at 380 nm. The
260 final Ca^{2+} traces were plotted using GraphPad Prism 9.0.
261
262 **Generation of the IMPA1 deletion in cell lines:** For generation of HEK293T-IMPA1$^{-/-}$ cell
263 line, the initial region of the coding sequence (CDS) (exon1) of the IMPA1 gene was targeted
264 by a pair of guide RNAs (sgRNAs) and deleted via CRISPR-Cas9 technology, then these
265 cells were transduced to stably express Muscarinic receptor M1. The sgRNAs targeting the
266 start of the CDS of IMPA1 gene, were designed via the crispr.mit.edu. The sequences of the
267 sgRNAs are as follows:
268 5' GGAGAACCACCTTGTTGGCCAAGCTGGAATGTAGTGGCGTTTTAGAGCTAGAAATAGCAAGTT 3'
269 5' GGAGAACCACCTTGTTGGGTAATATGGTACAGACACACGTTTTAGAGCTAGAAATAGCAAGTT 3'
270 These sgRNAs were cloned individually into humanized pgRNA plasmids (pgRNA-
271 humanized was a gift from Stanley Qi (Addgene plasmid # 44248). The cells were co-
272 transfected with the three plasmids (both the pgRNA humanized plasmids encoding the
273 sgRNAs and pLentiCas9 blast encoding for the Cas9 protein endonuclease from
274 *Streptococcus pyogenes*) and selected with Puromycin (2 µg/ ml) for 48 hours. Then the
275 genomic DNA was isolated and a Surveyor PCR was performed to check the occurrence of
276 the deletion. Once confirmed that the sgRNAs were able to target the exon 1 of IMPA1 gene,
277 the transfected cells were seeded in 96 wells as single cells and gradually expanded. After
278 selection via Surveyor PCR using Surveyor primers (primers flanking the region ought to be
279 deleted), a HEK293T cell line was selected which had showed only the shorter amplicon
280 (amplicon after deletion) in the Surveyor PCR. This HEK293T cell line was then expanded
281 and the expression of IMPA1 was checked by Western blotting using the anti-IMPA1
282 antibody. No corresponding bands for IMPA1 were observed, indicating that IMPA1 was
283 knocked out in this cell line. This HEK293T-IMPA1-/- cell line did not show any
284 morphological difference with respect to HEK293T cells and did not require inositol
285 supplementation in the media for maintenance.
286
287 **Western Blotting:** For estimating the expression of the IMPA1, cells were suspended in
288 appropriate volume of lysis buffer and kept on ice for lysis; 10 µl of it was used for Bradford
289 protein assay (BioRad) for quantification. Post quantification, equal amount of samples were

290 heated at 95°C with Laemli loading buffer for 5 min, then loaded and separated on 10%
291 SDS-PAGE gel. For estimating the expression of the muscarinic acetylcholine receptor
292 m1AchR, cells were pelleted and directly lysed by adding Laemmli's loading buffer and
293 repeated syringing with insulin syringes (31 gauge). Then the samples were heated at 95°C
294 for 5 min and loaded onto a pre-cast Polyacrylamide 4-12% gradient gel (Bolt, Invitrogen).
295 The proteins were then transferred onto a nitrocellulose membrane and then blocked with
296 10% Blotto (Santa Cruz Biotechnology) diluted in Tris Buffer Saline containing 0.1% Tween-
297 20 (0.1% TBST) for 40 minutes. Subsequently the membrane was incubated with the rabbit
298 anti-IMPA1 antibody (1:10000 diluted in 5% BSA in 0.1% TBST) (Abcam ab184165) or goat
299 anti-CHRM1 antibody (1 µg/ ml, diluted in 5% BSA in 0.1% TBST) (Abcam ab77098)
300 overnight at 4°C. For loading control, the blot was incubated with mouse anti-β-Tubulin
301 antibody (1:4000 diluted in 5% BSA in 0.1% TBST) (DSHB Hybridoma Product E7). The
302 blots were then washed thrice with 0.1% TBST and then incubated with the appropriate
303 HRP-conjugated secondary antibodies (1:10000 dilutions; Jackson Laboratories, Inc.) for 1.5
304 hrs. Post incubation with the secondary antibodies, the blot was washed thrice with 0.1%
305 TBST and developed using Clarity Western ECL substrate (Biorad) on a GEImageQuant
306 LAS 4000 system.The ImageJ software was used for the densitometric analysis of the blots.
307 Firstly, the background intensities were subtracted from the images using an average of
308 mean background intensities of a few ROIs adjacent to the band of interest. Then ROIs were
309 drawn around the bands of interest and the integrated density of each ROI was extracted
310 from the image. Finally, the ratio of the integrated density of the IMPase to that of the loading
311 control (β-Tubulin) was calculated.
312
313 **Calcium imaging for measuring transients:** For studying the effect of Li on the excitability
314 of cortical neurons, spontaneous calcium events (calcium transients) were measured in
315 D149 cortical neuronal cultures at 45 DIV for both untreated and Li treated neurons,
316 according to previously published lab protocol [44]. The neuronal cultures were washed
317 twice for 10 minutes with HBSS and then loaded with 4 µM of Fluo-4 AM (Molecular probes,
318 F14201) in HBSS having 0.002% Pluronic F-127 for 30 min at room temperature. Imaging
319 was performed for a time-span of 10 min using a 20X objective (N.A. 0.50) with a time
320 interval of 1 second at 488 nm illumination. The baseline measurement was recorded for a
321 period of 4 min to visualize the calcium transients. Then 10 µM Tetrodotoxin (TTX, Hellobio)
322 was added to abolish calcium transients and recorded for another 4 min. A dynamic region
323 of interest (ROI) was manually drawn around each neuronal soma; individual Ca^{2+} traces
324 were then obtained using the CellSens Dimensions software. The fluorescence intensity
325 value from each neuronal soma was normalized to the first baseline signal and the individual

326 traces were plotted using GraphPad Prism 9.0. The frequency of calcium transients was
327 measured manually from first-derivative filter traces.
328
329 **Post-hoc immunofluorescence for neuronal characterization:** Post-calcium imaging, the
330 neuronal cultures were washed thoroughly a few times with HBSS buffer and then fixed with
331 4% PFA dissolved in PBS for 20 mins. Post-fixation, the cultures were washed twice with
332 PBS for 5 min each and then permeabilized with 0.1% Triton-X (dissolved in PBS). The
333 cultures were then blocked with 5% BSA diluted in PBS, for 1 hr at room temperature.
334 Subsequently the neurons were incubated with the Primary antibodies diluted in 5% BSA in
335 PBS overnight at 4°C. Next day, the cultures were subjected to three washes with PBS (10
336 minutes each) to remove non-specifically bound primary antibody. Respective secondary
337 antibodies at a dilution of 1:300 in 5% BSA in PBS were used for incubation for 2 hours.
338 DAPI was used as a nuclear marker at a dilution of 1:1000.

Primary antibody	Source	Company	Catalogue number	Dilution
SOX1	Rabbit	Abcam	ab87775	1:400
Nestin	Mouse	Thermo Fisher	MA1-110	1:100
SOX2	Mouse	Thermo Fisher	MA1-014	1:500
Pax6	Rabbit	Thermo Fisher	MA1-109	1:100
GFAP	Rabbit	Abcam	ab7260	1:1000
MAP2	Chicken	Novus Biologicals	NB300-213	1:1000
CTIP2	Rat	Abcam	ab18465	1:800
Synapsin	Rabbit	Abcam	ab64581	1:200

339

Secondary antibody	Company	Catalogue number	Dilution
Alexa 488- Goat α-Rabbit IgG	Life Technology	A11034	1:300
Alexa 568- Goat α-Chicken IgG	Life Technology	A11041	1:300
Alexa 488-Goat α-Rat IgG	Life Technology	A11006	1:300
Alexa 568- Goat α-Mouse IgG	Life Technology	A11004	1:300

340

341 **RNA isolation, cDNA synthesis and Real-Time Quantitative PCR:** The total RNA was
342 extracted from HEK293T cells or mature neuronal cultures, in multiple biological replicates

using TRIzol (Ambion, Life Technologies) following manufacturer's protocol and thereby, quantified via Nanodrop 1000 spectrophotometer (Thermo Fisher Scientific). For cDNA synthesis, 1 µg of the RNA from each replicate was treated with DNase I (amplification grade, Thermo Fisher Scientific) and then incubated with Superscript II reverse transcriptase (Invitrogen) along with random hexamers and dNTPs. A no reverse transcription control sample was also included for each sample. Real-Time Quantitative PCR analysis was performed on an Applied Biosystems 7500 fast qPCR system using diluted cDNA samples and primers against genes of interest and GAPDH as internal controls. The C_t values obtained for different genes were normalized to those of GAPDH from the same sample. The relative expression levels were calculated using ΔC_t method, whereas the fold change was calculated using $\Delta\Delta C_t$ method. The primers used for qRT-PCR are listed in the Table 2.

LCMS based PIP and PIP_2 measurements: To validate whether the PH-PLCδ-GFP probe based imaging of PIP_2 in the HEK293T cells reflected the changes in PIP_2 level, mass spectrometry measurements of PIP_2 from the cells was carried out following existing lab protocols[64]. Reverse phase liquid chromatography was coupled with high sensitivity mass spectrometry (LCMS) and a Multiple Reaction Monitoring (MRM) method was employed to detect PIP_2 levels from the whole cells.

Lipid extraction—Equal number of cells from a single well of a 12 well plate (counted by a haemocytometer while seeding) were pelleted and then gently resuspended into 170 µl of 1X PBS in a 2 ml low-bind polypropylene centrifuge tube. To this, 750 µl of ice-cold quench mixture (MeOH/$CHCl_3$/1M HCl in the volumetric ratio of 484/242/23.55), followed by 15 µl of a pre-mixed ISD (Internal Standard) mixture containing 25 ng of 37:4 PIP [**PI4P 17:0/20:4 (LM-1901)]**, 25 ng of 37:4 PIP_2 [**PI 4,5P_2 17:0/20:4 (LM-1904)]** and 50 ng of 31:1 Phosphatidylethanolamine [**PE 17:0/14:1 (LM-1104)]** was added (All the lipid standards were procured from Avanti Lipids). For Carbamoylcholine chloride mediated PLC activation, cells were suspended in 85 µl of 1XPBS and then 85 µl of 20 µM Carbamoylcholine chloride (made in PBS) (final concentration – 10 µM) was added for 1 min at 37°C in shaking conditions. For the regeneration of PIP_2 post PLC mediated hydrolysis, 1 ml of ice-cold PBS was added to dilute the agonist Carbamoylcholine chloride and stop the stimulation. Cells were pelleted and washed and then resuspended in pre-warmed buffer (37°C) and kept for 15 mins for recovery (time given for regeneration of PIP_2). Post 15 mins of incubation, cells were pelleted and then resuspended in 170 µl of PBS, to which 750 µl of quench mixture and 15 µl of a pre-mixed ISD were added as stated previously. The mixture was vortexed and 725 µl of $CHCl_3$ and 170 µl of 2.4 M HCl were added. After vortexing again for 2 min at 1500 rpm, the phases were separated by centrifugation for 3 min at 1500 g. The lower

380 organic phase was then collected and added to fresh tubes containing 708 µl of Lower
381 Phase Wash Solution (LPWS; MeOH/1M HCl/$CHCl_3$ in the volumetric ratio of 235/245/15).
382 The tubes were then vortexed and spun at 1500 rpm again for 3 min to separate the phases.
383 The resultant lower organic phase was collected into a fresh tube and subjected to the
384 Derivatization reaction.

385 *Derivatization of Lipids*— 50 µl of 2M TMS-Diazomethane was added to the collected
386 organic phase (TMS-Diazomethane is toxic and is to be used with utmost precautions and
387 following safety guidelines). The reaction was allowed for 10 min at 600 rpm at room
388 temperature, post which 10 µl of Glacial acetic acid was added to quench the reaction. 500
389 µl of Post Derivatization Wash Solution (PDWS- $CHCl_3$/MeOH/H_2O in the volumetric ratio of
390 24/12/9; the upper phase was used) was then added to the sample, vortexed and spun
391 down at 1500 g for 3 min. The upper aqueous phase was discarded and the wash step was
392 repeated. To the final organic phase, 45 µl MeOH and 5 µl H_2O was added, mixed and spun
393 down. The samples were then dried in a SpeedVac at 400 rpm for 150 mins under vacuum
394 and 90 µl of MeOH was added to reconstitute the sample to a final volume of about 100µl.
395
396 *Chromatography and Mass spectrometry*—The chromatographic separation was performed
397 on an Acquity UPLC BEH300 C4 column (100 X 1.0 mm; 1.7 µm particle size - Waters
398 Corporation, USA) using a Waters Aquity UPLC system connected to an ABSCIEX 6500
399 QTRAP mass spectrometer for ion detection. All the samples were injected in duplicates and
400 the flow rate was set to 100 µl /min. Solvent gradients were set, starting from 55% Solvent A
401 (Water + 0.1% Formic Acid)- 45% Solvent B (Acetonitrile + 0.1% Formic acid) from 0-5 min;
402 then 45% B to 100% B from 5-10 min; 100% B was held from 10-15 min; between 15-16
403 min, 100% B was lowered to 45% B and held there till 20th min to re-equilibrate the column.
404 On the mass spectrometer, Neutral Loss Scans was employed during pilot standardization
405 experiments on biological samples to identify the parent ions that would lose neutral
406 fragments corresponding to 490 a.m.u and 382 a.m.u- these were indicative of PIP_2 and PIP
407 species respectively and likewise 155 a.m.u for PE species [64]. Thereafter, we quantified
408 PIP, PIP_2 and PE species in biological samples using the selective Multiple Reaction
409 Monitoring (MRM) method in the positive ion mode. Area under the peaks was calculated via
410 the Sciex MultiQuant software. For each run, area under the peak for each species of PIP_2,
411 PIP and PE was normalized to PIP_2, PIP and PE internal standard peak respectively.
412 Thereafter, the sum of normalized areas for all the species of PIP_2 or PIP was taken and
413 divided by the sum of normalized areas for all the species of PE in each of the biological
414 samples to account for differences in total phospholipid extracted across samples. The MRM

415 mass pairs used for PIP, PIP_2 and PE species identification and quantification are listed
416 below:
417
418
419

Q1 Mass (Da)	Q3 Mass (Da)	Dwell time (msec)	ID	DP (volts)	EP (volts)	CE (volts)	CXP (volts)
1041.5	551.5	35	32_0 PIP2	60	11	37	15
1039.5	549.5	35	32_1 PIP2	60	11	37	15
1069.5	579.5	35	34_0 PIP2	60	11	37	15
1067.5	577.5	35	34_1 PIP2	60	11	37	15
1065.5	575.5	35	34_2 PIP2	60	11	37	15
1103.5	613.5	35	37_4 PIP2	60	11	37	15
995.5	613.5	35	37_4 PIP	140	12	29	12
1097.5	607.5	35	36_0 PIP2	60	11	37	15
1095.5	605.5	35	36_1 PIP2	60	11	37	15
1093.5	603.5	35	36_2 PIP2	60	11	37	15
1091.5	601.5	35	36_3 PIP2	60	11	37	15
1089.5	599.5	35	36_4 PIP2	60	11	37	15
1125.5	635.5	35	38_0 PIP2	60	11	37	15
1123.5	633.5	35	38_1 PIP2	60	11	37	15
1121.5	631.5	35	38_2 PIP2	60	11	37	15
1119.5	629.5	35	38_3 PIP2	60	11	37	15
1117.5	627.5	35	38_4 PIP2	60	11	37	15
1115.5	625.5	35	38_5 PIP2	60	11	37	15
933.5	551.5	35	32_0 PIP	140	12	29	12
931.5	549.5	35	32_1 PIP	140	12	29	12
961.5	579.5	35	34_0 PIP	140	12	29	12
959.5	577.5	35	34_1 PIP	140	12	29	12
957.5	575.5	35	34_2 PIP	140	12	29	12
989.5	607.5	35	36_0 PIP	140	12	29	12
987.5	605.5	35	36_1 PIP	140	12	29	12
985.5	603.5	35	36_2 PIP	140	12	29	12
983.5	601.5	35	36_3 PIP	140	12	29	12
981.5	599.5	35	36_4 PIP	140	12	29	12
1017.5	635.5	35	38_0 PIP	140	12	29	12
1015.5	633.5	35	38_1 PIP	140	12	29	12

1013.5	631.5	35	38_2 PIP	140	12	29	12
1011.5	629.5	35	38_3 PIP	140	12	29	12
1009.5	627.5	35	38_4 PIP	140	12	29	12
1007.5	625.5	35	38_5 PIP	140	12	29	12
706.5	551.5	35	PE 32_0	140	12	29	12
704.5	549.5	35	PE 32_1	140	12	29	12
734.5	579.5	35	PE 34_0	140	12	29	12
732.5	577.5	35	PE 34_1	140	12	29	12
730.5	575.5	35	PE 34_2	140	12	29	12
762.5	607.5	35	PE 36_0	140	12	29	12
760.5	605.5	35	PE 36_1	140	12	29	12
758.5	603.5	35	PE 36_2	140	12	29	12
756.5	601.5	35	PE 36_3	140	12	29	12
754.5	599.5	35	PE 36_4	140	12	29	12
790.5	635.5	35	PE 38_0	140	12	29	12
788.5	633.5	35	PE 38_1	140	12	29	12
786.5	631.5	35	PE 38_2	140	12	29	12
784.5	629.5	35	PE 38_3	140	12	29	12
782.5	627.5	35	PE 38_4	140	12	29	12
780.5	625.5	35	PE 38_5	140	12	29	12
690.5	535.5	65	PE(31:1)	140	12	29	12

The other mass spectrometer parameters were:
ESI voltage: +5100-5200 V; Source Temperature: 300 C, Curtain Gas (CUR): 35-37, Ion Source Gas 1 (GS1):15-20, Ion Source Gas 2 (GS2): 15-20.

RNA sequencing and transcriptomic analysis: RNA extracted from mature neurons (45DIV with and without Li treatment) and NSCs (wild-type, Li treated wild-type, IMPA knock-out and Li treated IMPA knock-out) as mentioned above was submitted for paired-end sequencing. Quality check and sequencing was carried out at the NCBS Sanger sequencing facility using Illumina Hiseq 2500 system. Single stranded RNA sequencing libraries were prepared for sequencing using NEBNext® Ultra™ II Directional RNA Library Prep with Sample Purification Beads (Catalog no-E7765L). Paired-end reads, (125 base pair for each neuronal sample and 100 base pair for each NSC samples) was obtained after sequencing. Post adapter trimming, FastQC was used to check the quality of reads. The reads were then aligned to human genome (GRCh38) using hisat2-build and hisat2-align module. The module for single strand sequencing was used in the Hisat-2 protocol. The output generated

436 in the bam format, was further used to obtain the counts of each of the individual gene using
437 HT-Seq pipeline. The differential expression of genes was then calculated using DeSeq2.
438 GO annotation analysis was done using the DAVID tool.
439
440 **Sampling and statistical analysis:** Each experiment was performed unblinded on different
441 biological groups with multiple biological replicates. No statistical analysis was done a priori
442 to determine the sample sizes. For the calcium imaging experiments, quantification was from
443 a minimum of 100 cells for all genotypes from multiple dishes of each type. For the PIP_2
444 probe experiments, approximately 50 cells were taken for the quantitative analysis.
445 Statistical significance was computed using Student's unpaired t-test to check for differences
446 in means between samples of different genotypes. Two-way ANOVA with post hoc Tukey's
447 pairwise comparison was used for the grouped analysis. All statistical analyses were
448 performed on Graph Pad Prism (version 9) and schematic representations were created with
449 biorender.com.

450

451 # Results

452 **An *in vivo* model system to study the impact of Li on PLC induced PIP_2 turnover**

453 In order to study the turnover of PIP_2 following receptor activated Phospholipase C (PLC)
454 turnover, we created a cell line which heterologously expressed two components. To
455 stimulate high levels of PLC activity, we expressed the human Muscarinic acetylcholine
456 receptor (m1AchR) encoded by the gene *CHRM1*; previous studies have shown that
457 activation of heterologously expressed m1AchR results in high rates of PIP_2 hydrolysis
458 leading to IP_3 production [29, 30]. To monitor the levels of PIP_2 at the plasma membrane we
459 expressed the PH-domain of PLC-δ fused to green fluorescent protein (PH-PLCδ::GFP).
460 This probe binds to PIP_2 and in imaging experiments; its relative distribution between the
461 plasma membrane and the cytosol has been used by us and others to monitor plasma
462 membrane PIP_2 levels [31, 32]. A cell line expressing both m1AchR and PH-PLCδ::GFP can
463 therefore be used to stimulate PLC and monitor the turnover of PIP_2 at the plasma
464 membrane. We generated stable HEK293T cell lines expressing m1AchR (control-M1) and
465 PH-PLCδ::GFP was transiently expressed in those cells (Fig 1B); when stimulated with the
466 m1AchR agonist Carbamoyl choline (carbachol: Cch), the levels of PH-PLCδ::GFP at the
467 plasma membrane drop following which they gradually recover back towards pre-stimulation
468 levels (Fig 1C). The changes in plasma membrane PIP_2 was quantified as the ratio of
469 fluorescence intensity of the PH-PLCδ::GFP probe at the plasma membrane to its
470 fluorescence intensity in the underlying cytosol in the same part of the cell (Fig 1C). As a

471 positive control, for our assay to monitor PIP_2 regeneration following PLC activation, we
472 used shRNA to deplete Nir2; Nir2 (PITPNM1/RdgBαI) encodes for a phosphatidylinositol
473 transfer protein required for the resynthesis of PIP_2 following PLC stimulation [33–35]. Under
474 our experimental conditions, we found that depletion of Nir2 in our HEK293T reporter line
475 resulted in a decreased rate in the recovery of plasma membrane PIP_2 levels following
476 stimulation with carbachol (Fig 1D,E).
477

478 To measure the effect of Li treatment on PIP_2 resynthesis, we incubated our reporter line
479 with 1 mM Li; this concentration of LiCl was used in our experiments since the therapeutic
480 range for Li medication in BD patients was 0.75 to1.5 mEq/L [36]. Following Li treatment, we
481 stimulated the cells with carbachol and compared the dynamics of plasma membrane PIP_2
482 levels with that in non-Li treated cells. We found that in Li treated cells the rate with which
483 PIP_2 levels at the plasma membrane recovered to pre-stimulation levels was significantly
484 slower than in untreated controls (Fig 1 F,G). These findings strongly suggest that treatment
485 with Li results in a reduction in the rate of PIP_2 resynthesis following PLC stimulation.
486

487 In an alternative approach, we quantified total cellular PIP_2 mass using liquid
488 chromatography coupled with tandem mass spectrometry (LC-MS/MS) at three distinct time
489 points- corresponding to the basal state, one minute post-stimulation of PLC via carbachol
490 addition (hydrolysis of PIP_2) state and post-stimulation (recovery of PIP_2) state. From these
491 experiments, the time for recovery of PIP_2 (to pre-stimulation levels) was standardized at 15
492 minutes post stimulation with carbachol (Fig 1H). Using these conditions, we compared the
493 total PIP_2 mass between untreated cells and those treated with Li. We found that the mass
494 of PIP_2 in Li treated cells during the recovery phase was lower in Li treated cells compared
495 to controls (Fig 1I); likewise, the level of phosphatidylinositol phosphate (PIP) in Li treated
496 cells was also lower during the recovery phase (Fig 1J). Thus, Li treatment lowers the
497 recovery of PIP and PIP_2 levels following PLC activation.
498

499 **Chronic Li treatment reduces PLC dependent intracellular Ca^{2+} mobilization**

500 A key outcome of agonist triggered PIP_2 hydrolysis by PLC activation is intracellular Ca^{2+}
501 signalling [11]. Since we noted a reduction in the turnover of PIP_2 following Li treatment, we
502 tested the impact of Li treatment on intracellular Ca^{2+} levels $[Ca^{2+}]_I$. Using the control-M1 cell
503 line, we monitored $[Ca^{2+}]_I$ under both resting conditions as well as stimulation with carbachol,
504 an agonist of m1AchR. Cells were incubated in 1 mM Li prior to the experiment: basal $[Ca^{2+}]_I$
505 were no different between treated and untreated cells (Fig 2A). Stimulation of untreated cells
506 with carbachol evoked a rise in $[Ca^{2+}]_I$ which then decayed back to resting levels (Fig 2B). In

507 cells treated with Li, the carbachol induced rise in $[Ca^{2+}]_I$ was reduced compared to that seen
508 in untreated cells (Fig 2C). Receptor activated PLC mediated Ca^{2+} signalling is a biphasic
509 process with two components, and an initial release of Ca^{2+} from intracellular stores followed
510 by store-operated influx of Ca^{2+} into the cell from the extracellular medium [37]. We
511 performed experiments to separately monitor each of these components. During the initial
512 phase of the assay, carbachol stimulation was performed in the presence of zero
513 extracellular Ca^{2+}, thus selectively monitoring release of Ca^{2+} from intracellular stores (Fig
514 2D,E). Following this, the extracellular solution was supplemented with Ca^{2+} and the influx of
515 Ca^{2+} into the cytoplasm was monitored (Fig 2D,F). This analysis revealed that in Li treated
516 cells both intracellular Ca^{2+} release (Fig 2E) as well as the subsequent store operated Ca^{2+}
517 influx into cells was reduced (Fig 2F) compared to Li untreated controls. This reduction in
518 receptor activated release of Ca^{2+} from intracellular stores was not due to a reduction in the
519 size of intracellular Ca^{2+} stores as emptying of stores by the application of thapsigargin
520 resulted in equivalent rises in $[Ca^{2+}]_I$ in Li treated cells and untreated controls (Fig 2G,H).
521
522 According to the "inositol depletion hypothesis" [19], Li can restrict the available cytoplasmic
523 inositol pool available for phosphatidylinositol (PI) (and thence PIP_2) resynthesis by inhibiting
524 IMPase- thereby, lowering down the synthesis of the pool of PIP_2 that is required for PLC
525 mediated generation of DAG and IP_3. This cytoplasmic inositol pool can also be replenished
526 by transport of inositol from the extracellular medium via plasma membrane inositol
527 transporters (summarized in [38]). This implies that if a deficit in the available pool of
528 cytosolic inositol is responsible for the attenuated calcium signalling in Li treated cells, this
529 might be rescued by supplementation of the extracellular medium with inositol. We grew
530 HEK293T cells in an inositol rich DMEM media (inositol concentration is ca. 28 mg/litre;
531 which is similar to the inositol concentration in the cerebrospinal fluid [39–41]). These cells
532 were subjected to Li treatment and agonist induced Ca^{2+} influx was quantified. As controls in
533 this experiment, we used Li treated control-M1cells grown in DMEM not supplemented with
534 inositol. As in previous experiments, we found that when cells were grown in DMEM, Li
535 treatment resulted in a reduction of agonist induced Ca^{2+} influx (Fig 2I,J). However, when Li
536 treatment was done on cells grown in inositol supplemented DMEM, the Li induced reduction
537 in Ca^{2+} influx was rescued compared to that seen in cells grown under equivalent Li
538 treatment but in DMEM not supplemented with inositol (Fig 2I,J), compared to Li non-treated
539 cells.
540
541

542 **IMPA1 is required for the effect of Li on PIP_2 resynthesis and agonist mediated**
543 **calcium signalling**
544 IMPase, the enzyme that dephosphorylates inositol monophosphate to generate myo-inositol
545 has been proposed as a direct target of the action of Li, inhibiting its activity [42, 43]. There
546 are two genes encoding IMPase in the human genome *IMPA1* and *IMPA2* of which *IMPA1* is
547 the predominant isoform expressed in HEK293T cells. To test the requirement of *IMPA1*, we
548 generated a HEK293T cell line in which *IMPA1* was deleted by CRISPR/Cas9 genome
549 editing (Supp. Fig 3A); m1AchR was expressed in these cells by lentiviral transduction;
550 these cells will be denoted as $IMPA1^{-/-}$-M1. Western blot analysis of the $IMPA1^{-/-}$ line showed
551 the complete absence of the IMPA1 protein (Fig 3A), IMPA2 levels were not altered (Supp.
552 Fig 3B) and the levels of m1AchR protein was comparable between control-M1 cells and
553 $IMPA1^{-/-}$-M1 cells (Supp. Fig 3C,D). We tested the effect of Li treatment on $IMPA1^{-/-}$-M1
554 compared to untreated $IMPA1^{-/-}$-M1 cells. This analysis revealed that the rate of regeneration
555 of PIP_2 at the plasma membrane was unchanged in $IMPA1^{-/-}$-M1 cells subjected to Li
556 treatment, compared to untreated $IMPA1^{-/-}$-M1 cells (Fig 3B). In addition, the rate of PIP_2
557 regeneration was much slower in $IMPA1^{-/-}$-M1 cells compared to control-M1 cells (Fig 3C).
558 These observations suggest that ability of Li to slow PIP_2 resynthesis following PLC
559 activation requires an intact IMPA1.
560
561 We also analysed $IMPA1^{-/-}$-M1 cells for receptor activated Ca^{2+} influx, following Li treatment;
562 this was not altered compared to untreated $IMPA1^{-/-}$-M1 cells (Fig 3D,E); in the same
563 experiment, treatment of control-M1 cells with Li resulted in a big reduction in agonist
564 activated Ca^{2+} influx. We also analyzed the two phases of receptor activated Ca^{2+} influx and
565 found that while release of $[Ca^{2+}]_I$ from stores was not affected by Li treatment in $IMPA^{-/-}$-M1
566 cells (Fig 3F,G), the reduction of SOCE previously noted on Li treatment in control-M1 cells
567 was still present (Fig 3F,H). When we expressed IMPA1 cDNA in the $IMPA1^{-/-}$-M1 cells, the
568 receptor activated Ca^{2+} influx became similar to that of control-M1 cells (Fig 3J,K). These
569 observations suggest that intact IMPA1 is required for the ability of Li treatment to reduce
570 intracellular Ca^{2+} release following PLC activation.
571
572 **Li reduces excitability in human cortical neurons**
573 To test the relevance of our findings to human cortical neurons whose activity presumably
574 underlies the therapeutic effect of Li in bipolar disorder patients, we generated human
575 forebrain cortical neurons from induced pluripotent stem cells (iPSC) *in vitro* [44]. We
576 differentiated forebrain cortical neurons from neural stem cells (NSC) derived from an Indian
577 control iPSC line, D149 (Fig 4A) [45]. The generated NSCs expressedpreviously described

578 markers characteristic of NSC such as Nestin, SOX1, SOX2 and PAX6 (Fig 4B) and when
579 differentiated, expressed the neuronal marker MAP2;a proportion of cells in the culture
580 expressed the glial marker GFAP (Fig 4C). When these NSCs were differentiated into
581 cortical neurons, they exhibited spontaneous $[Ca^{2+}]_i$ elevations, referred to as transients, that
582 increase as a function of age *in vitro* [44, 46]. We measured $[Ca^{2+}]_i$ transients from such
583 neuronal cultures at 45 *days in vitro* (DIV 45) and quantified their frequency. We observed
584 that the frequency of $[Ca^{2+}]_i$ transients was decreased following Li treatment (1 mM) for 10
585 days (Fig 4D,E). We also measured changes in $[Ca^{2+}]_i$ following stimulation with carbachol in
586 DIV45 cortical neurons treated with Li. In our cultures carbachol stimulation results in a rise
587 in $[Ca^{2+}]_i$ that peaks before gradually decaying towards the baseline; in Li treated cultures the
588 peak of this response was reduced (Fig 4F,G). We also performed experiments to measure
589 Ca^{2+} mobilization from internal stores; these revealed that carbachol activated release of
590 Ca^{2+} in Li treated neurons was reduced compared to those that were untreated (Fig 4H-J).
591 By contrast there was only a modest difference in thapsigargin mediated rise in $[Ca^{2+}]_i$
592 between Li treated and untreated cortical neurons (Supp. Fig 4A-C). These observations
593 suggest that both neuronal excitability as well as PLC mediated Ca^{2+} signalling is attenuated
594 in cortical neurons following Li treatment.
595

596 **Li treatment induces transcriptional changes in pathways involved in neuronal**
597 **excitability**

598 To understand the molecular mechanisms underlying the reduced excitability following Li
599 treatment in human iPSC derived cortical neurons, we performed a transcriptomic analysis
600 comparing untreated 45 DIV neurons and Li treated 45 DIV neurons (Fig 5A). Differentially
601 expressed genes were obtained using DeSeq2; a cut-off of log_2FC change greater than 0.2
602 was used along with a p-value and FDR significance at less than 0.05 were considered.
603 Using these criteria, 335 upregulated and 361 downregulated genes were obtained (Table 1
604 S1,S2). Gene Ontology (GO) analysis of the KEGG pathway showed substantial enrichment
605 for genes annotated as being involved in calcium signalling or in glutamatergic synapse
606 (Table 1 S3). In addition, GO KEGG analysis of the downregulated gene set also showed
607 enrichment for several other categories of neurotransmission and neuromodulation related
608 pathways (cholinergic, GABAergic, dopaminergic, glutamatergic and serotonergic) (Table 1
609 S2) (Fig 5B).
610

611 Since GO analysis revealed an enrichment in Ca signalling genes, we analysed molecular
612 mechanisms through which Li might downregulate neuronal Ca signalling and hence
613 excitability. There are multiple molecular mechanisms by which neuronal calcium signalling

614 is modulated [47] including voltage gated Ca channels and receptor activated Ca signalling,
615 a mechanism used by several neurotransmitters and neuromodulators. Using the
616 transcriptomic data, we tested the likely contribution of each of these mechanisms to the
617 effects of Li in our model system.
618
619 Physiological and pharmacological evidence suggests that the $[Ca^{2+}]_I$ transients seen during
620 neuronal development arise from the activity of voltage gated calcium channels (VGCC) [48]
621 and this also seems to underlie the $[Ca^{2+}]_I$ transients seen in our experiments when human
622 iPSC are differentiated into cortical neurons [44][this study]. To understand the mechanism
623 by which Li could reduce the frequency of $[Ca^{2+}]_I$ transients we specifically studied the
624 expression of genes encoding VGCC. Our transcriptomic analysis suggested that expression
625 of genes encoding several subunits of VGCC might be downregulated (Table 1 S3). We
626 experimentally tested the expression of genes for *CACNA1A, CACNA1B, CACNA1C,*
627 *CAC1A1D* and *CACN1A1E* by qRT-PCR analysis; this showed that the expression of
628 CACNA1A,B,C,D were all downregulated in Li treated DIV45 neurons compared to controls
629 (Fig 5C) whereas CACNA1E was unchanged. In the same analysis, there was no
630 downregulation in transcripts for *SCN1A (Nav1.1)* or *SCN9A (Nav7.1)* that encode the brain
631 enriched, a-subunit of voltage gated sodium channels, involved in plasma membrane
632 depolarization that trigger VGCC dependent $[Ca^{2+}]_I$ transients (Fig 5C).
633
634 Glutamate is a key excitatory neurotransmitter in the human central nervous system,
635 exerting its effects through both metabotropic and ionotropic mechanisms [14] and changes
636 in $[Ca^{2+}]_I$ isa key mechanism in glutamate signalling in the human brain. Our qRT-PCR
637 analysis of transcript levels of genes encoding key components in the glutamate signalling
638 system in Li treated neurons revealed that transcript levels for metabotropic glutamate
639 receptors (*GRM1, GRM3, GRM5, GRM7*) and the ionotropic glutamate receptors (*GRIA1,*
640 *GRIA2, GRIN1, GRIN2A, GRIN2B*) were downregulated (Fig 5D).
641
642 Many neurotransmitters and modulators transduce signal via G-protein coupled, PLC
643 mediated store-operated Ca^{2+} influx [49]. Key molecular components of this pathway include
644 the IP_3 receptor, ER Ca^{2+} sensor STIM and the Ca influx channel ORAI; we found that
645 transcript levels of *PLCb4, ITPR2, STIM1* and *ORAI2* were all downregulated in Li treated
646 neurons compared to controls (Fig 5E).
647
648 **Mechanisms of Li induced transcriptional changes**
649 To understand the mechanisms underlying Li induced transcriptome changes we analysed
650 the likely transcriptional control mechanisms. For this we used the htFtarget database that

has information on all human transcription factors (TFs) and the genes they control, tissue specific TF-target information, data on TFs for non-coding RNA and information on co-regulation for a target gene and its TFs [50]. TFs controlling genes differentially expressed in Li treated neurons (DIV 45) were identified from the htFtarget database. Out of 650 up regulated genes in Li treated neurons, 587 were identified as associated with one or more TFs in this database. Likewise, out of 525 downregulated genes, 333 genes were linked to a TF. 485 and 323 unique TFs were identified that control the upregulated and downregulated genes respectively. We then further looked for transcription factors that control differentially expressed genes that are involved in calcium signalling (Table1 S3) (Fig 5F). Of the upregulated genes, only RYR receptor was associated with three different transcription factors (CTCF, SPI1 and USF1) that could control its expression. On the other hand, several genes involved in calcium signalling that were downregulated were controlled by transcription factors. Expression of *CACNA1C, CACNA1D, CAMK2B, CAMK4, CHRM3, GRIN1, ITPR2, RYR3, SCN9A* and *SLC2A13* genes is regulated by transcription factors. Of these *ITPR2* and *CAMK2B* are regulated by 10 different TFs, while *CACNA1D, CHRM3, RYR3, SCN9A and SLC2A13* are regulated by single transcription factor (Fig 5G). This suggests that some of the genes that are differentially expressed in Li treated neurons are under transcriptional control which can be a direct or indirect effect of Li treatment.

Discussion

Li is a monovalent ion with a remarkable therapeutic effect in the management of BPAD. However only a proportion of human patients with BPAD respond to treatment and the reasons underlying this variable response to Li remains unknown. In part this is due to a lack of clear understanding on the mechanisms of action of Li in the brain. Although many molecular targets of Li have been described in the literature, their role in mediating the action of Li *in vivo* has not been directly tested.

One of the earliest cellular effects described for Li is its ability to slow Phosphoinositide turnover in neural cells [51] and it has been proposed that the consequent slowing of neurotransmitter activated neuronal excitability may underlie the effectiveness of the compound[19] in managing BPAD. Since Li inhibits the enzyme IMPA1, one long-standing proposal is that the application of Li to cells disrupts the receptor activated PIP_2 cycle and its downstream effect on $[Ca^{2+}]_I$ signallingleading to reduced neuronal excitability. However, there has not been a direct test of the model that the ability of Li to modulate inositol turnover and $[Ca^{2+}]_I$ signalling *in vivo* requires the *IMPA1* gene product.

687

688 In this study, we found that in the application of Li to human cells resulted in a reduction in
689 $[Ca^{2+}]_I$ signalling following PLC activation. This reduction in $[Ca^{2+}]_I$ was underpinned by a
690 reduction in the release of Ca^{2+} from intracellular stores although the size of stores itself was
691 not altered by Li treatment, implying that Li affects the release mechanism. During PLC
692 activation, the principal mechanism by which Ca^{2+} is released is via the IP_3 receptor;
693 however, we found that the transcript levels for this gene were not altered by Li treatment
694 (Supp. Fig 2C). Thus, it seems likely that Li treatment affects IP_3 receptor activation, perhaps
695 by altering IP_3 production during receptor mediated PLC stimulation, a process that requires
696 adequate levels of the substrate for PLC, PIP_2. During this study we found that Li treatment
697 slows that rate of synthesis of PIP_2, the substrate from which PLC produces IP_3 and this
698 observation likely provides an explanation for the reduced intracellular Ca^{2+} release
699 phenotype seen following PLC stimulation.

700

701 We generated a cell line in which IMPA1 was deleted and found that in the absence of
702 IMPA1, Li was unable to exert its effects on both $[Ca^{2+}]_I$ signalling and PIP_2 resynthesis
703 during receptor activated PLC signalling. These findings imply that an intact IMPA1 is
704 required for the action of Li on these processes. Consistent with this idea, we noted that
705 receptor activated $[Ca^{2+}]_I$ signalling (Fig 3D,E) and the rate of PIP_2 resynthesis (Fig 3C)
706 following PLC activation was reduced in IMPA1$^{-/-}$ cells without Li treatment and in brain
707 cells[42]leading to the therapeutic effects of Li.

708

709 IMPA1 is an enzyme that dephosphorylates inositol 1-phosphate to generate inositol. Hence
710 biological effects resulting from Li inhibition could arise either from an accumulation of the
711 substrate or a deficiency of product. Indeed, Li treatment in rodent models has shown both
712 an elevation of inositol 1-phosphate levels as well as a modest reduction in inositol levels
713 [52][53]. In our analysis, we found that the lowered $[Ca^{2+}]_I$ influx following receptor activation
714 in human cells could be rescued by supplementation of the culture medium with inositol. This
715 observation implies that the signalling defect arising from Li inhibition of IMPA1 is a
716 consequence of inositol depletion rather than an accumulation of the substrate inositol 1-
717 phosphate. During the PLC activated PIP_2 cycle, inositol generated by the action of IMPA1 is
718 condensed with cytidine diphosphate diacylglycerol to form phosphatidylinositol[54] which is
719 then sequentially phosphorylated to generate PIP_2. Consistent with a role for reduced
720 inositol levels in the $[Ca^{2+}]_I$ signalling phenotype resulting from Li treatment, we found that
721 the resynthesis of PIP_2 was also slowed by treatment of wild type cells with Li. Together, our
722 data provide compelling evidence that Li treatment results in inhibition of IMPA1, a depletion
723 of the inositol pool leading to a reduced rate of PIP_2 resynthesis during PLC signalling.

724 When Li is used to treat BPAD in human patients, presumably it acts by reducing the
725 excitability of neurons in the cerebral cortex. In this study, we tested the effect of Li treatment
726 on human forebrain cortical neuronal cultures differentiated from iPSC. Consistent with
727 previous reports [55], we found that treatment of human forebrain cortical neurons with
728 therapeutically relevant concentrations of Li reduced the frequency of $[Ca^{2+}]_I$ transients that
729 are underpinned by voltage gated Ca^{2+} channel (VGCC) activity [44]. Since acute application
730 of Li does not affect $[Ca^{2+}]_I$ transients (Supp. Fig 4D,E), it seems unlikely that Li affects
731 neuronal excitability by directly inhibiting the VGCC. However, VGCC mediated $[Ca^{2+}]_I$
732 transients are activated by neuronal action potentials which themselves are triggered by
733 activation of post-synaptic G-protein coupled receptors that bind neurotransmitters. Several
734 of these receptors (mGluR1, mGluR5, mAchR and 5HT-2A) when bound to their respective
735 neurotransmitter ligand, use PLC activation as part of their signalling mechanism. Thus, Li
736 could influence neuronal excitability by modulating signalling through such PLC linked
737 receptors. In support of this hypothesis, this study we found that in human forebrain cortical
738 neurons, Li application diminished the elevations of $[Ca^{2+}]_I$ triggered by application of the
739 mAchR ligand carbachol (Fig 4 F-I). Thus, a key mechanism by which Li modulates neuronal
740 excitability may be through downregulation of neurotransmitter signalling through PLC linked
741 GPCRs.
742
743 Given the extended timeframe over which Li exerts its therapeutic effect it has been
744 proposed that in addition to directly impacting cellular biochemistry, transcriptional
745 mechanisms may play a role in its biological effects. SOCE that occurs downstream of
746 receptor activated PLC signalling has been shown to regulate transcription in neurons
747 [reviewed in [56] and a proposed target of Li, GSK-3β exerts its signalling effects via the
748 transcriptional regulator β-catenin [57]. In a transcriptomic analysis of human forebrain
749 cortical neurons, we found that Li treatment on a clinically relevant time and concentration
750 range results in a large transcriptional response. Bioinformatics analysis of Li treated
751 neurons did not reveal features of β-catenin dependent transcriptome changes and qRT-
752 PCR analysis of selected β-catenin regulated genes did not reveal any alteration in their
753 transcript levels in Li treated cells relative to controls (Supp. Fig 5A,B). Further, a
754 comparison of differentially expressed genes from genetic ablation of GSK-3β or the
755 chemical inhibition of this molecule[58] to the dataset of Li induced differential gene
756 expression (this study) revealed only a minimal overlap in the identity of genes altered in
757 both datasets (Supp. Fig 5F). Consistent with this, treatment of HEK293 cells with GSK-3β
758 inhibitor did not result in any alteration in receptor mediated $[Ca^{2+}]_I$ (Supp. Fig 5D,E).
759 Therefore, it seems that the transcriptome changes induced by Li treatment occur through a
760 non-GSK-3β/ β-catenin mediated mechanism. Likewise, a comparison of Li induced

differential gene expression (this study) to that elicited by genetic inhibition of SOCE [59, 60] also revealed only a modest overlap of genes that were differentially regulated (Supp Fig 4F,G). Therefore, it is likely that Li exerts transcriptional changes in neurons independent of its effects on SOCE.

Our analysis of the Li induced transcriptome changes in human forebrain cortical neurons however provide an insight into the mechanisms by which Li might mediate its effects both in cultured forebrain cortical neurons and also its clinical effects. We found that the levels of three of the four subunits of VGCC were downregulated in Li treated cells and this could explain in part the ability of Li to reduce $[Ca^{2+}]_I$ transients in forebrain cortical neurons in culture. A key feature of mania in BPAD patients is heightened neural activity manifested behaviorally, EEG and fMRI studies and presumably Li exerts its therapeutic effect through downregulating this neural activity. Glutamate is the principle excitatory neurotransmitter in the brain [14] and consistent with this we found that transcripts for multiple glutamate receptor subtypes were downregulated in forebrain cortical neurons treated with Li. These included multiple subunits of the metabotropic, AMPA and NMDA subtypes of the glutamate receptor family. Downregulation of these will likely contribute to reducing neural activity following Li treatment manifest clinically as behavioral improvement. Overall, this study demonstrates that the effects of Li on neuronal Ca^{2+}signalling are mediated through an IMPA dependent step and involves a large transcriptional response that downregulates molecular processes that are required for neuronal excitability. The link between Li and transcriptional responses are unclear although studies in yeast have shown that treatment with Li is associated with changes in the transcriptome that also includes changes in inositol biosynthesis.

Acknowledgements: This work was supported by the Department of Atomic Energy, Government of India, under Project Identification No. RTI 4006, the Department of Biotechnology, Government of India through the Accelerator Program for Discovery in Brain Disorders (BT/PR17316/MED/31/326/2015), the Pratiksha Trust and a Wellcome-DBT India Alliance Senior Fellowship to PR (IA/S/14/2/501540). We thank the NCBS Imaging, Mass spectrometry, Genomics, High performance computing, Stem cell and Biosafety facilities for support.

Conflict of Interest:

The authors declare no competing interests**.**

Bibliography

1. Toker L, Bersudsky Y, Plaschkes I, Chalifa-Caspi V, Berry GT, Buccafusca R, et al. Inositol-related gene knockouts mimic lithium's effect on mitochondrial function. Neuropsychopharmacology. 2014;39:319–328.

2. Osby U, Brandt L, Correia N, Ekbom a, Sparén P. Excess mortality in bipolar and unipolar disorder in Sweden. Arch Gen Psychiatry. 2001;58:844–850.

3. Lopez AD, Murray CC. JL. The global burden of disease , 1990 – 2020. Nat Med. 1998;4:1241–1243.

4. Geddes JR, Burgess S, Hawton K, Jamison K, Goodwin GM. Long-term lithium therapy for bipolar disorder: systematic review and meta-analysis of randomized controlled trials. Am J Psychiatry. 2004;161:217–222.

5. Cipriani A, Hawton K, Stockton S, Geddes JR. Lithium in the prevention of suicide in mood disorders: updated systematic review and meta-analysis. Bmj. 2013;3646:1–13.

6. Hou L, Heilbronner U, Degenhardt F, Adli M, Akiyama K, Akula N, et al. Genetic variants associated with response to lithium treatment in bipolar disorder: A genome-wide association study. The Lancet. 2016;387:1085–1093.

7. Manchia M, Adli M, Akula N, Ardau R, Aubry J-M, Backlund L, et al. Assessment of Response to Lithium Maintenance Treatment in Bipolar Disorder: A Consortium on Lithium Genetics (ConLiGen) Report. PLoS One. 2013;8:e65636.

8. Haggarty SJ, Karmacharya R, Perlis RH. Advances toward precision medicine for bipolar disorder: mechanisms & molecules. Mol Psychiatry. 2021;26:168–185.

9. Roux M, Dosseto A. From direct to indirect lithium targets: a comprehensive review of omics data. Metallomics. 2017;9:1326–1351.

10. Harwood a J. Lithium and bipolar mood disorder: the inositol-depletion hypothesis revisited. Mol Psychiatry. 2005;10:117–126.

11. Berridge MJ. Inositol trisphosphate and calcium signalling mechanisms. Biochimica et Biophysica Acta (BBA) - Molecular Cell Research. 2009;1793:933–940.

12. Wasserman MJ, Corson TW, Sibony D, Cooke RG, Parikh S V., Pennefather PS, et al. Chronic lithium treatment attenuates intracellular calcium mobilization. Neuropsychopharmacology. 2004;29:759–769.

13. Yang YR, Kang D-S, Lee C, Seok H, Follo MY, Cocco L, et al. Primary phospholipase C and brain disorders. Adv Biol Regul. 2016;61:80–85.

14. Reiner A, Levitz J. Glutamatergic Signaling in the Central Nervous System: Ionotropic and Metabotropic Receptors in Concert. Neuron. 2018;98:1080–1098.

15. Cockcroft S, Raghu P. Topological organisation of the phosphatidylinositol 4,5-bisphosphate-phospholipase C resynthesis cycle: PITPs bridge the ER-PM gap. Biochemical Journal. 2016;473:4289–4310.

16. Allison, J.H. SMA. Reduced inositol in rat brain on lithium injection. Nat New Biol. 1971. 1971.

17. Allison JH, Blisner ME, Holland WH, Hipps PP, Sherman WR. Increased brain myo-inositol 1-phosphate in lithium-treated rats. BiochemBiophys Res Commun. 1976;71:664–670.

18. Allison JH, Blisner ME, Holland WH, Hipps PP, Sherman WR. Increased brain myo-inositol 1-phosphate in lithium-treated rats. BiochemBiophys Res Commun. 1976;71:664–670.

19. Berridge MJ, Downes CP, Hanley MR. Neural and developmental actions of lithium: a unifying hypothesis. Cell. 1989;59.

20. Colantuoni C, Lipska BK, Ye T, Hyde TM, Tao R, Leek JT, et al. Temporal dynamics and genetic control of transcription in the human prefrontal cortex. Nature. 2011;478:519–523.

21. Schubert CR, O'Donnell P, Quan J, Wendland JR, Xi HS, Winslow AR, et al. BrainSeq: Neurogenomics to Drive Novel Target Discovery for Neuropsychiatric Disorders. Neuron. 2015;88:1078–1083.

22. Ohnishi T, Ohba H, Seo KC, Im J, Sato Y, Iwayama Y, et al. Spatial expression patterns and biochemical properties distinguish a second myo-inositol monophosphatase IMPA2 from IMPA1. Journal of Biological Chemistry. 2007;282:637–646.

23. Sherman WR, Leavitt AL, Honchar MP, Hallcher LM, Phillips BE. Evidence that Lithium Alters Phosphoinositide Metabolism: Chronic Administration Elevates Primarily d-myo-Inositol-1-Phosphate in Cerebral Cortex of the Rat. J Neurochem. 1981;36:1947–1951.

24. Soares JC, Dippold CS, Mallinger AG. Platelet membrane phosphatidylinositol-4,5-bisphosphate alterations in bipolar disorder--evidence from a single case study. Psychiatry Res. 1997;69:197–202.

25. Soares JC, Mallinger AG, Dippold CS, Frank E, Kupfer DJ. Platelet membrane phospholipids in euthymic bipolar disorder patients: are they affected by lithium treatment? Biol Psychiatry. 1999;45:453–457.

26. Soares JC, Mallinger AG, Dippold CS, Forster Wells K, Frank E, Kupfer DJ. Effects of lithium on platelet membrane phosphoinositides in bipolar disorder patients: a pilot study. Psychopharmacology (Berl). 2000;149:12–16.

27. Cryns K, Shamir A, Van Acker N, Levi I, Daneels G, Goris I, et al. IMPA1 is essential for embryonic development and lithium-like pilocarpine sensitivity. Neuropsychopharmacology. 2008;33:674–684.

28. Sjoholt G, Gulbrandsen AK, Lovlie R, Berle JO, Molven A, Steen VM. A human myo-inositol monophosphatase gene (IMPA2) localized in a putative susceptibility region for bipolar disorder on chromosome 18p11.2: genomic structure and polymorphism screening in manic- depressive patients. Mol Psychiatry. 2000;5:172–180.

29. Parker EM, Kameyama K, Higashijima T, Ross EM. Reconstitutively active G protein-coupled receptors purified from baculovirus-infected insect cells. J Biol Chem. 1991;266:519–527.

30. Raghu P, Habib S, Hasnain SE, Kasan G. Development of a functional assay for Ca^{2+}release activity of IP<inf>3</inf>R and expression of an IP<inf>3</inf>R gene fragment in the baculovirus-insect cell system. Gene. 1997;190.

31. Várnai P, Balla T. Visualization of phosphoinositides that bind pleckstrin homology domains: calcium- and agonist-induced dynamic changes and relationship to myo-[3H]inositol-labeled phosphoinositide pools. J Cell Biol. 1998;143:501–510.

32. Chakrabarti P, Kolay S, Yadav S, Kumari K, Nair A, Trivedi D, et al. A dPIP5K dependent pool of phosphatidylinositol 4,5 bisphosphate (PIP2) is required for G-protein coupled signal transduction in Drosophila photoreceptors. PLoS Genet. 2015;11:e1004948.

33. Chang C-L, Liou J. Phosphatidylinositol 4,5-Bisphosphate Homeostasis Regulated by Nir2 and Nir3 Proteins at Endoplasmic Reticulum-Plasma Membrane Junctions. J Biol Chem. 2015;290:14289–14301.

34. Kim S, Kedan A, Marom M, Gavert N, Keinan O, Selitrennik M, et al. The phosphatidylinositol-transfer protein Nir2 binds phosphatidic acid and positively regulates phosphoinositide signalling. EMBO Rep. 2013;14:891–899.

35. Kim YJ, Guzman-Hernandez M-L, Wisniewski E, Balla T. Phosphatidylinositol-Phosphatidic Acid Exchange by Nir2 at ER-PM Contact Sites Maintains Phosphoinositide Signaling Competence. Dev Cell. 2015;33:549–561.

36. Francis J, Hamzeh RK, Lantin-Hermoso MR. Lithium toxicity-induced wide-complex tachycardia in a pediatric patient. Journal of Pediatrics. 2004;145:235–240.

37. Prakriya M, Lewis RS. Store-Operated Calcium Channels. Physiol Rev. 2015;95:1383–1436.

38. Balla T. Phosphoinositides: Tiny Lipids With Giant Impact on Cell Regulation. Physiol Rev. 2013;93:1019–1137.

39. Nixon DA. Cerebrospinal fluid inositol and its rise in post-mortem specimens. J Physiol. 1955;129:272–280.

40. Swahn C -G. Gas chromatographic-mass spectrometric determination of myo-inositol in human cerebrospinal fluid. J Neurochem. 1985;45:331–334.

41. Shetty HU, Holloway HW, Schapiro MB. Cerebrospinal fluid and plasma distribution of myo-inositol and other polyols in Alzheimer disease. Clin Chem. 1996;42:298–302.

42. Hallcher LM, Sherman WR. The effects of lithium ion and other agents on the activity of myo- inositol-1-phosphatase from bovine brain. J Biol Chem. 1980;255:10896–10901.

43. V S, P V, QT D, RA A, V S, PD P, et al. 7Li nuclear-magnetic-resonance study of lithium binding to myo-inositolmonophosphatase. Eur J Biochem. 1996;240:288–291.

44. Sharma Y, Saha S, Joseph A, Krishnan H, Raghu P. In vitro human stem cell derived cultures to monitor calcium signaling in neuronal development and function [version 1; peer review: 3 approved]. Wellcome Open Res. 2020;5:16:doi: 10.12688/wellcomeopenres.15626.1. eCollection.

45. Iyer S, Bhatia P, Rao M, Mukherjee O. Developing two reference control samples for the Indian population. Stem Cell Res. 2018;30:38–42.

920 46. Akhtar BM, Bhatia P, Acharya S, Sharma S, Sharma Y, Bhuvanendran Nair Suseela
921 Devi A, et al. A human stem cell resource to decipher the biochemical and cellular
922 basis of neurodevelopmental defects in Lowe syndrome. Biol Open. 2022;11.

923 47. Berridge MJ. Neuronal calcium signaling. 1998;21:13–26.

924 48. Rosenberg SS, Spitzer NC. Calcium Signaling in Neuronal Development. Cold Spring
925 HarbPerspect Biol. 2011;3:a004259–a004259.

926 49. Moccia F, Zuccolo E, Soda T, Tanzi F, Guerra G, Mapelli L, et al. Stim and Orai
927 proteins in neuronal Ca(2+) signaling and excitability. Front Cell Neurosci. 2015;9.

928 50. Zhang Q, Liu W, Zhang HM, Xie GY, Miao YR, Xia M, et al. hTFtarget: A
929 Comprehensive Database for Regulations of Human Transcription Factors and Their
930 Targets. Genomics Proteomics Bioinformatics. 2020;18:120–128.

931 51. Berridge MJ, Downes CP, Hanley MR. Lithium amplifies agonist-dependent
932 phosphatidylinositol responses in brain and salivary glands. Biochem J.
933 1982;206:587–595.

934 52. Sherman WR, Leavitt AL, Honchar MP, Hallcher LM, Phillips BE. Evidence that
935 Lithium Alters Phosphoinositide Metabolism: Chronic Administration Elevates
936 Primarily d-myo-Inositol-1-Phosphate in Cerebral Cortex of the Rat. J Neurochem.
937 1981;36:1947–1951.

938 53. Sade Y, Toker L, Kara NZ, Einat H, Rapoport S, Moechars D, et al. IP3 accumulation
939 and/or inositol depletion: two downstream lithium's effects that may mediate its
940 behavioral and cellular changes. Transl Psychiatry. 2016;6:e968.

941 54. Lykidis A, Jackson PD, Rock CO, Jackowski S. The Role of CDP-Diacylglycerol
942 Synthetase and Phosphatidylinositol Synthase Activity Levels in the Regulation of
943 Cellular Phosphatidylinositol Content. 1997;272:33402–33409.

944 55. Mertens J, Wang Q-W, Kim Y, Yu DX, Pham S, Yang B, et al. Differential responses
945 to lithium in hyperexcitable neurons from patients with bipolar disorder. Nature.
946 2015;527:95–99.

947 56. Mitra R, Hasan G. Store-operated Ca 2+ entry regulates neuronal gene expression
948 and function. CurrOpinNeurobiol. 2022;73.

949 57. He R, Du S, Lei T, Xie X, Wang Y. Glycogen synthase kinase 3β in tumorigenesis and
950 oncotherapy (Review). Oncol Rep. 2020;44:2373–2385.

951 58. Chen X, Wang R, Liu X, Wu Y, Zhou T, Yang Y, et al. A Chemical-Genetic Approach
952 Reveals the Distinct Roles of GSK3α and GSK3β in Regulating Embryonic Stem Cell
953 Fate. Dev Cell. 2017;43:563-576.e4.

954 59. Gopurappilly R, Deb BK, Chakraborty P, Hasan G. Stable STIM1 Knockdown in Self-
955 Renewing Human Neural Precursors Promotes Premature Neural Differentiation.
956 Front Mol Neurosci. 2018;11.

957 60. Dhanya SK, Hasan G. Purkinje Neurons with Loss of STIM1 Exhibit Age-Dependent
958 Changes in Gene Expression and Synaptic Components. J Neurosci. 2021;41:3777–
959 3798.

960 61. Mukherjee O, Acharya S, Rao M. Making NSC and Neurons from Patient-Derived
961 Tissue Samples. Methods Mol Biol, vol. 1919, 2019. p. 9–24.

962 62. Peh GSL, Lang RJ, Pera MF, Hawes SM. CD133 expression by neural progenitors
963 derived from human embryonic stem cells and its use for their prospective isolation.
964 Stem Cells Dev. 2009;18:269–282.

965 63. Grynkiewicz G, Poenie M, Tsien RY. A new generation of Ca2+ indicators with greatly
966 improved fluorescence properties. J Biol Chem. 1985;260:3440–3450.

967 64. Sharma S, Mathre S, Ramya V, Shinde D, Raghu P. Regulates Plasma-Membrane
968 PIP 3 Turnover and Regulates Plasma-Membrane PIP 3 Turnover and Insulin
969 Signaling. CellReports. 2019;27:1979-1990.e7.

970

971

972 ## Figure legends:

973

974 **Figure 1- An *in vivo* model system to study the impact of Li on PLC induced PIP_2**
975 **turnover:**

976 (A) The Phosphatidylinositol bisphosphate (PIP_2) cycle. (B) Schematic representation of an
977 *in vivo* system elucidating the role of Nir2 and m1AchR in the PIP_2 cycle and the PH-
978 PLCδ::GFP probe binding to the PIP_2 at the plasma membrane. (C) The PH-PLCδ::GFP
979 probe translocates to the cytoplasm and back to the plasma membrane, corresponding to
980 the hydrolysis and regeneration of PIP_2 respectively (control-M1; HEK293T cells expressing
981 m1AchR). (D, E) Nir2 depletion leads to a delayed regeneration of PIP_2 at the plasma
982 membrane. Changes in membrane localization of the PH-PLCδ::GFP probe after Cch
983 stimulation (denoted by the ↑), are quantified via the fluorescence intensity ratio of the
984 plasma membrane and the cytosol (PM/ Cyt) at various times. This ratio is normalized to the
985 first time-point and the mean ± SD is plotted (from three experiments each performed in
986 replicates) for control cells (orange line, n =33), and for cells treated with Nir2 shRNA (blue
987 line, n =28). (F, G) Rate of regeneration of PIP_2 at the plasma membrane is shown for
988 control-M1 cells (HEK293T cells expressing m1AchR) subjected to lithium treatment,
989 compared to untreated cells. Mean ± SD is plotted from four experiments, each performed in
990 replicates (untreated cells- orange line, n = 58; cells treated with Li- green line, n =53).
991 [Scale Bar- 20 μM]. (H) Total PIP_2 levels recovered after various time intervals post
992 stimulation with Cch.
993 (I,J) Total PIP_2 and PIP levels using LCMS from whole cell lipid extract of untreated and
994 lithium treated cells (n=6 for both).
995 [Statistical test: (H) one-way ANOVA with post hoc Tukey's multiple pairwise comparisons.
996 *p value < 0.05; **p value <0.01; ***p value < 0.001; ****p value < 0.0001 and (I,J) Multiple
997 unpaired t test. *p value < 0.05; **p value <0.01; ***p value < 0.001].

998

999 **Figure 2- Chronic Lithium treatment reduces PLC dependent intracellular Ca^{2+}**
1000 **mobilization:**
1001 (A) Basal $[Ca^{2+}]_I$, calculated in nM using Grynkiewicz equation, is unchanged in control-M1
1002 cells due to lithium treatment (untreated cells- represented by orange, n = 133; cells treated
1003 with Li -represented by green line, n =156). (B-C) PLC dependent calcium mobilization is
1004 decreased in lithium treated cells. Quantification is done from multiple experiments, each
1005 with replicates (untreated cells (orange), n =133; cells treated with Li (green), n =156). (D-F)
1006 In zero Ca^{2+} buffer, agonist dependent calcium mobilization is reduced and subsequent
1007 Store Operated Calcium Entry (SOCE) is also decreased in lithium treated cells.
1008 Quantification: untreated cells (orange), n =145; cells treated with Li (green), n =146. (G-H)
1009 Intracellular store measured by Tg, is unaltered by lithium treatment. Quantification:
1010 untreated cells (orange), n =114; cells treated with Li (green), n =118. (I-J) Inositol
1011 supplementation reversed the lithium mediated decrease in intracellular Ca^{2+} release.
1012 Quantification: untreated cells (orange), n =98; cells treated with Li (green), n =114, cells
1013 treated with Li and high inositol (blue), n =104.
1014 [Statistical tests: (C,E,F) Student's unpaired t test. *p value < 0.05; **p value <0.01; ***p
1015 value < 0.001; ****p value < 0.0001 and (J) one-way ANOVA with post hoc Tukey's multiple
1016 pairwise comparisons. *p value < 0.05; **p value <0.01; ***p value < 0.001; ****p value <
1017 0.0001].
1018
1019

1020 **Figure 3- IMPA1 is required for the effect of Li on PIP_2 resynthesis and agonist**
1021 **mediated Ca^{2+} signalling:**
1022 (A) Western blot confirmation of IMPA1 knock-out cells. (B) Lithium does not alter the rate of
1023 regeneration of PIP_2 at the plasma membrane in the IMPA1$^{-/-}$-M1 cells (HEK293T-IMPA1$^{-/-}$
1024 cells expressing m1AchR), as monitored by the changes in the translocation of the PH-
1025 PLCδ::GFP probe. Mean ± SD is plotted from four experiments, each performed in replicates
1026 (IMPA1$^{-/-}$ cells without Li treatment- blue line, n =50; IMPA1$^{-/-}$ cells treated with Li- purple
1027 line, n =47). (C) PIP_2 turnover post PLC stimulation in control-M1 (HEK293T cells expressing
1028 m1AchR) cells compared to IMPA1$^{-/-}$-M1 cells [control-M1 cells- orange line, n =50, IMPA1$^{-/-}$-
1029 M1 cells- blue line, n =51]. (D,E) Cch mediated calcium release in IMPA1$^{-/-}$-M1 cells are not
1030 altered by lithium. Quantification: control-M1 cells (orange), n =126; control-M1 cells treated
1031 with Li (green), n =127, IMPA1$^{-/-}$-M1 cells without Li treatment (blue), n =132; IMPA1$^{-/-}$-M1
1032 cells treated with Li (purple), n =112. (F-H) In zero Ca^{2+} buffer, agonist dependent calcium
1033 mobilization is unaltered, but subsequent Store Operated Calcium Entry (SOCE) is
1034 decreased in lithium treated IMPA1$^{-/-}$-M1 cells. Quantification: IMPA1$^{-/-}$-M1 cells without Li

1035 treatment (blue), n =179; IMPA1$^{-/-}$-M1 cells treated with Li (purple), n =193. (I) Western blot
1036 showing IMPA1 expression via lentiviral transduction of cDNA in IMPA1 knock-out cells.
1037 (J,K) IMPA1 expression via lentiviral transduction of cDNA in IMPA1$^{-/-}$-M1 cells cells
1038 reversed the decreased intracellular Ca^{2+} release. Quantification: control-M1 cells (orange),
1039 n =155; IMPA1$^{-/-}$-M1 cells (light blue), n =143, IMPA1$^{-/-}$-M1 cells + IMPA1 cDNA (dark blue),
1040 n =162.
1041 [Statistical tests: (E,K) one-way ANOVA with post hoc Tukey's multiple pairwise
1042 comparisons. *p value < 0.05; **p value <0.01; ***p value < 0.001; ****p value < 0.0001 and
1043 (H) Student's unpaired t test. *p value < 0.05; **p value <0.01; ***p value < 0.001; ****p value
1044 < 0.0001].
1045
1046
1047 **Figure 4- Lithium reduces excitability in human cortical neurons:**
1048 (A) Overview of expansion and differentiation process of the D149 lineage Neural Stem Cells
1049 (NSCs) and the cortical neurons. (B) Characterization of NSCs via immunocytochemistry of
1050 known markers like Nestin, Sox2, Sox1 and Pax6. (C) The mature cortical neurons are
1051 characterized via immunocytochemistry of markers like MAP2, CTIP2 and GFAP (Astrocytes
1052 marker) [Scale Bar – 25 μM]. (D) $[Ca^{2+}]_I$ traces from individual cells (soma; Y-axis shows ΔF
1053 and X-axis is time in seconds. The baseline was recorded for 270 secs followed by addition
1054 of 10 μM Tetrodotoxin (TTX) (as indicated by the arrows) to block Ca^{2+} transients. Transients
1055 are higher in frequency in the neuronal cultures without lithium treatment, compared to the
1056 treated cultures. The number of spikes/ 270 secs are counted from individual soma and
1057 plotted, each dot representing events from a single soma. (E) Data is plotted from multiple
1058 experiments, each done with biological replicates (untreated neurons (orange), n =114;
1059 neurons treated with Li (green), n =113). (F-G) Cch dependent calcium mobilization was
1060 decreased in lithium treated neuronal cultures (DIV 45). Quantification: untreated neurons
1061 (orange), n =97; neurons treated with Li (green), n =106. (H-J) Decrease in the Cch
1062 dependent calcium mobilization as well as in Store Operated Calcium Entry (SOCE) cells in
1063 lithium treated neuronal cultures (DIV 45). Quantification: untreated neurons (orange), n
1064 =154; neurons treated with Li (green), n =156.
1065 [Statistical tests: (E,G,I,J) Student's unpaired t test . *p value < 0.05; **p value <0.01; ***p
1066 value < 0.001; ****p value < 0.0001].
1067
1068
1069 **Figure 5- Lithium treatment induces transcriptional changes in pathways involved in**
1070 **neuronal transmission:**

1071 (A) Volcano plot showing expression of genes altered due to lithium treatment in human
1072 cortical neuronal cultures 45 DIV (p value <0.05, p adj value <0.01). (B) The GO KEGG
1073 pathway enrichment analysis for downregulated genes. (C-E) Quantitative analysis showing
1074 several genes related to voltage calcium channels (C), Glutamatergic pathway (D) and
1075 calcium homeostasis (E), are downregulated in cortical neurons (DIV 45) due to lithium
1076 treatment. (F) Transcription factors that regulate genes involved in calcium signalling were
1077 identified using hTFtarget database. The graph represents number of calcium signalling
1078 genes controlled by each transcription factor in the lithium treated neurons. (G) The graph
1079 represents number of transcription factors that control each gene involved in calcium
1080 signalling.
1081 [Statistical tests: (C,D,E) Multiple unpaired t test . *p value < 0.05; **p value <0.01; ***p value
1082 < 0.001].
1083
1084
1085 ## Table legends:
1086
1087 **Table 1:**
1088 **Table 1 S1: List of upregulated genes in Li treated neurons DIV 45.**
1089 The table shows Gene ID (ENSEMBL ID), Gene names, base Mean, $\log_2$ fold change, p
1090 value, p adjusted value and gene description (as derived from Deseq2 analysis)
1091 **Table 1 S2: List of downregulated genes in Li treated neurons DIV 45.**
1092 The table shows Gene ID (ENSEMBL ID), Gene names, base Mean, $\log_2$ fold change, p
1093 value, p adjusted value and gene description (as derived from Deseq2 analysis)
1094 **Table 1 S3: List of genes involved in calcium signalling.**
1095 The table shows Gene ID (ENSEMBL ID), Gene names, base Mean, $\log_2$ fold change, p
1096 value, p adjusted value and gene description (as derived from Deseq2 analysis)
1097 **Table 1 S4: GO pathway analysis for the upregulated genes in Li treated neurons DIV**
1098 **45.**
1099 The table shows GO-Category, GO-Term, Count, Percentage of genes, p value, Gene IDs
1100 (ENSEMBL IDs), Fold Enrichment and its significance (as derived from DAVID GO analysis).
1101 **Table 1 S5: GO pathway analysis for the downregulated genes in Li treated neurons**
1102 **DIV 45.**
1103 The table shows GO-Category, GO-Term, Count, Percentage of genes, p value, Gene IDs
1104 (ENSEMBL IDs), Fold Enrichment and its significance (as derived from DAVID GO analysis).
1105
1106 **Table 2:**

1107 List of primers used for qRT-PCR.
1108 The table shows the gene names and the primer sequence in 5' to 3' orientation.
1109

1110 Supplementary Figure legends:

1111

1112 **Supplementary Figure 1- An in vivo model system to study the impact of Li on PLC**
1113 **induced PIP_2 turnover:**
1114 (A) Nir2 downregulation due to shRNA. (B) Rate of regeneration of PIP_2 at the plasma
1115 membrane is shown for control-M1 cells transfected with Nir2 shRNA, compared to control-
1116 M1 cells transfected with scrambled shRNA. Mean ± SD is plotted from two experiments,
1117 each performed in replicates control cells (orange line, n =18), and for cells treated with Nir2
1118 shRNA (blue line, n =21). (C,D) Relative abundance of the PIP_2 and PIP species shown, as
1119 detected by LC-MS/MS (MRM method in the positive mode).
1120 [Statistical test: (A) Student's unpaired t test. *p value < 0.05; **p value <0.01; ***p value <
1121 0.001.]
1122

1123 **Supplementary Figure 2- Chronic Lithium treatment reduces PLC dependent**
1124 **intracellular Ca^{2+} mobilization:**
1125 (A-C) Expression studies were done to check whether the decrease in SOCE in the lithium
1126 treated HEK293T cells was due to alteration of the genes involved in SOCE. No significant
1127 change occurred in terms of the expression of ITPR, STIM and ORAI in HEK293T cells due
1128 to lithium treatment.
1129
1130

1131 **Supplementary Figure 3- IMPA1 is required for the effect of Li on PIP_2 resynthesis and**
1132 **agonist mediated Ca^{2+} signalling:**
1133 (A) The starting region of the CDS of *IMPA1* gene is targeted by guide RNAs (gRNAs) and
1134 deleted by spCas9; (B) IMPA2 expression is not altered in these knock-out cells. *IMPA1* is
1135 the predominant gene in HEK293T cells that encodes for IMPase. (C, D) Western blot
1136 showing that both the reporter lines (control-M1 and $IMPA1^{-/-}$-M1 cells) exhibit similar
1137 expression of the m1AchR and thereby should achieve similar PC stimulation due to same
1138 concentration of Cch.
1139
1140

1141 **Supplementary Figure 4- Lithium reduces excitability in human cortical neurons:**

1142 (A-C) Intracellular store measured by Tg, is unaltered by lithium treatment in human cortical
1143 neurons. Quantification: untreated neurons (orange), n =145; neuronal cultures treated with
1144 Li (green), n =145. (D) $[Ca^{2+}]_I$ traces from individual cells (DIV 30 neurons) pre- and post-
1145 acute lithium treatment (1 mM Li for 5 mins) (soma; Y-axis shows ΔF and X-axis is time in
1146 seconds). Initially, the baseline was recorded for 300 secs- then 1 mM Li was added to the
1147 bath, incubated for 5 minutes and then recorded again for 300 secs. (E) The number of
1148 spikes/ 270 secs are counted from individual soma and plotted, each dot representing
1149 events from a single soma. Quantification- neurons before Li treatment (orange), n =41;
1150 neurons treated with Li for 5 mins (green), n =38. (F) The number of differentially expressed
1151 genes that are common between lithium treated neurons and in mouse Purkinje neurons
1152 where STIM1 is knocked out. (G) The number of differentially expressed genes that are
1153 common between lithium treated neurons and in neuronal progenitor cells where STIM1 is
1154 knocked down.
1155 [Statistical tests: (B,C) Student's unpaired t test . *p value < 0.05; **p value <0.01; ***p value
1156 < 0.001; ****p value < 0.0001].
1157
1158
1159 **Supplementary Figure 5- Lithium treatment induces transcriptional changes in**
1160 **pathways involved in neuronal transmission:**
1161 (A,B) Transcriptomic analyses were done to check whether lithium treatment in mature
1162 neuronal affected genes involved in the Wnt signalling/ GSK-3β pathway. No significant
1163 alteration occurred in terms of the expression of the relevant genes due to lithium treatment.
1164 (C) Western blot showing CHIR99021 (an inhibitor of GSK-3β) treatment led to the high
1165 expression of β-Catenin, one of the targets of GSK-3β destruction complex. (D,E) Inhibition
1166 of GSK-3β by CHIR99021 did not alter agonist mediated Ca^{2+} release. Quantification:
1167 untreated cells (orange), n =116; cells treated with CHIR99021 (blue), n =118. (F) The
1168 number of differentially expressed genes that are common between lithium treated neurons
1169 and in mouse ES cells (Embryonic Stem cells) where GSK-3β is inhibited.
1170

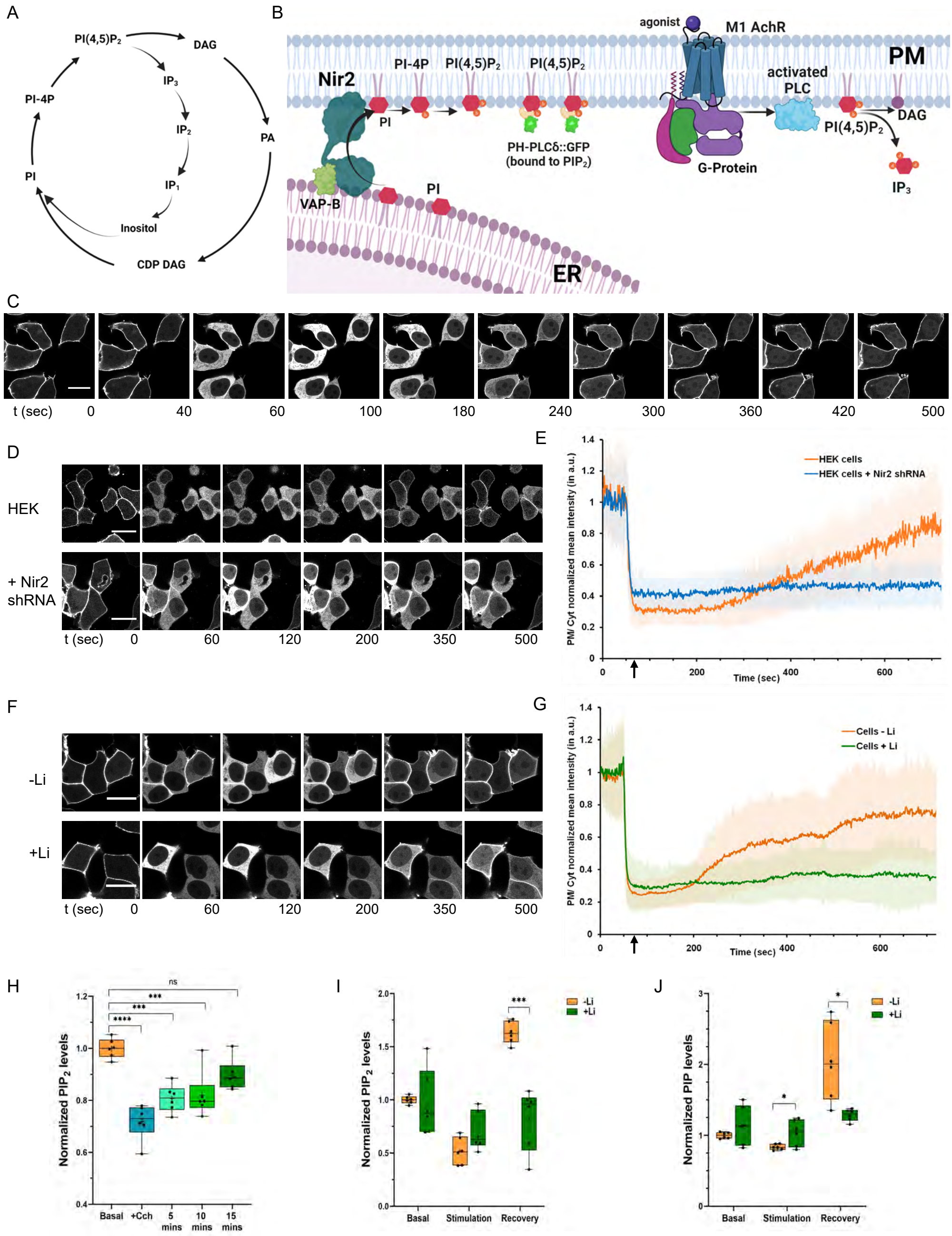

Saha Figure 1

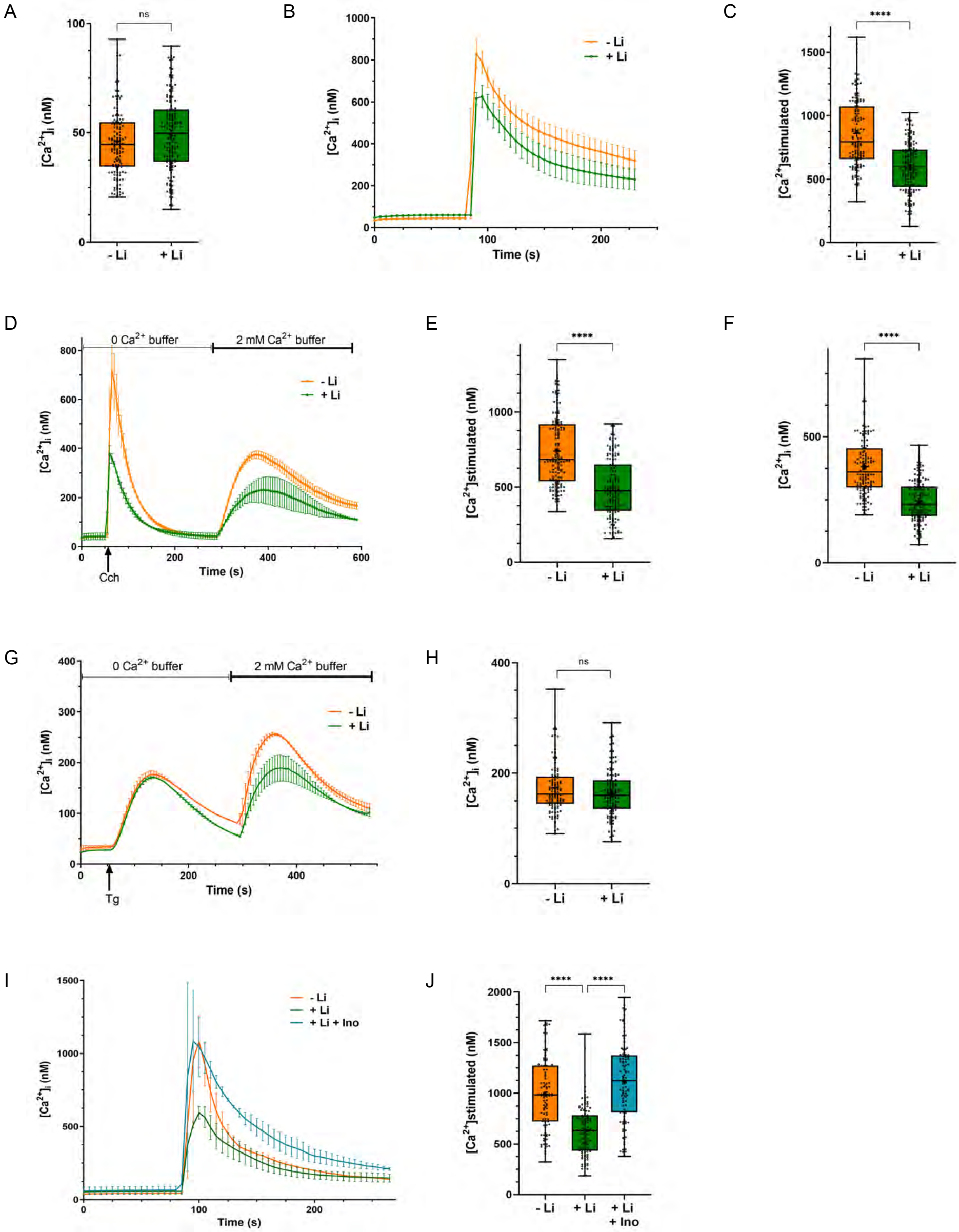

Saha Figure 2

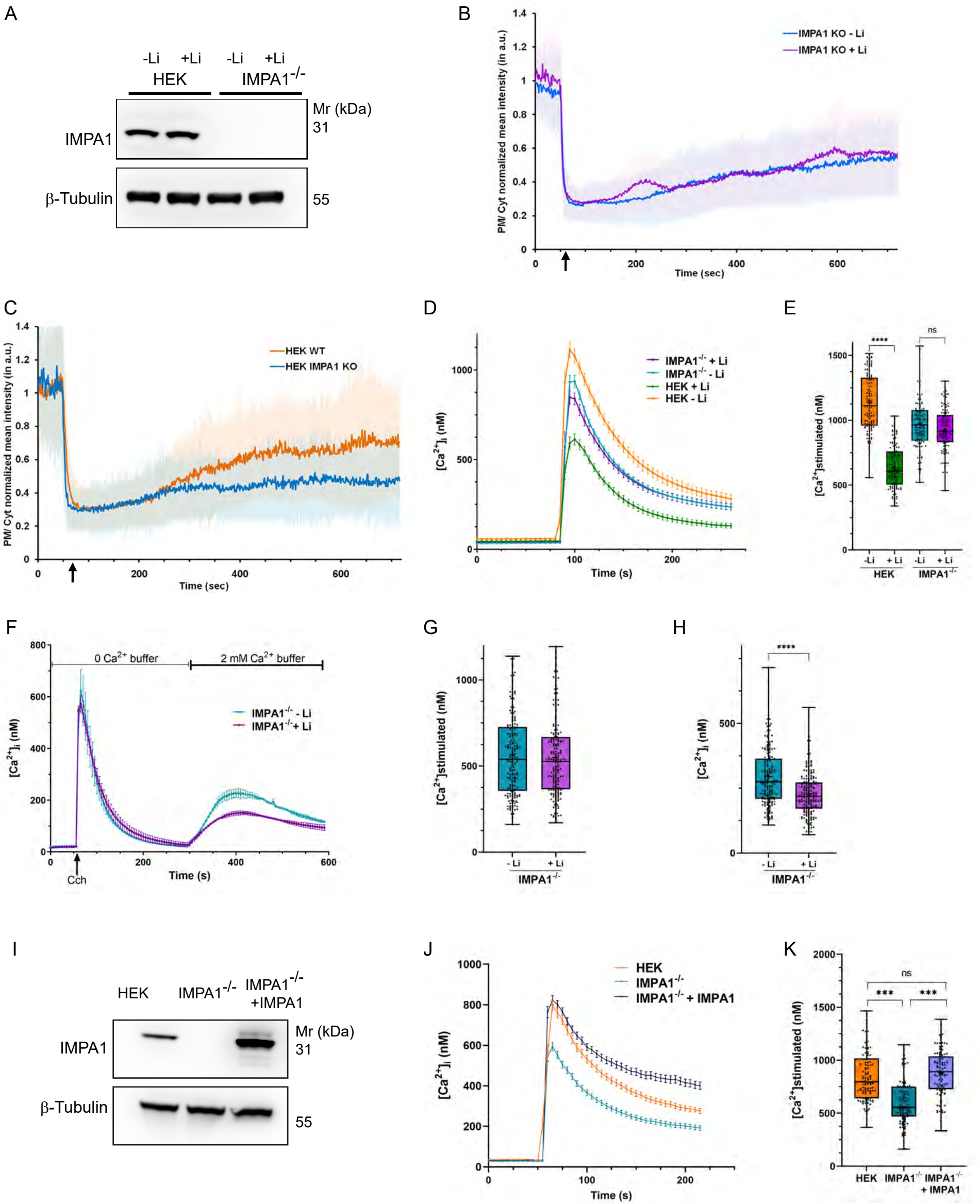

Saha Figure 3

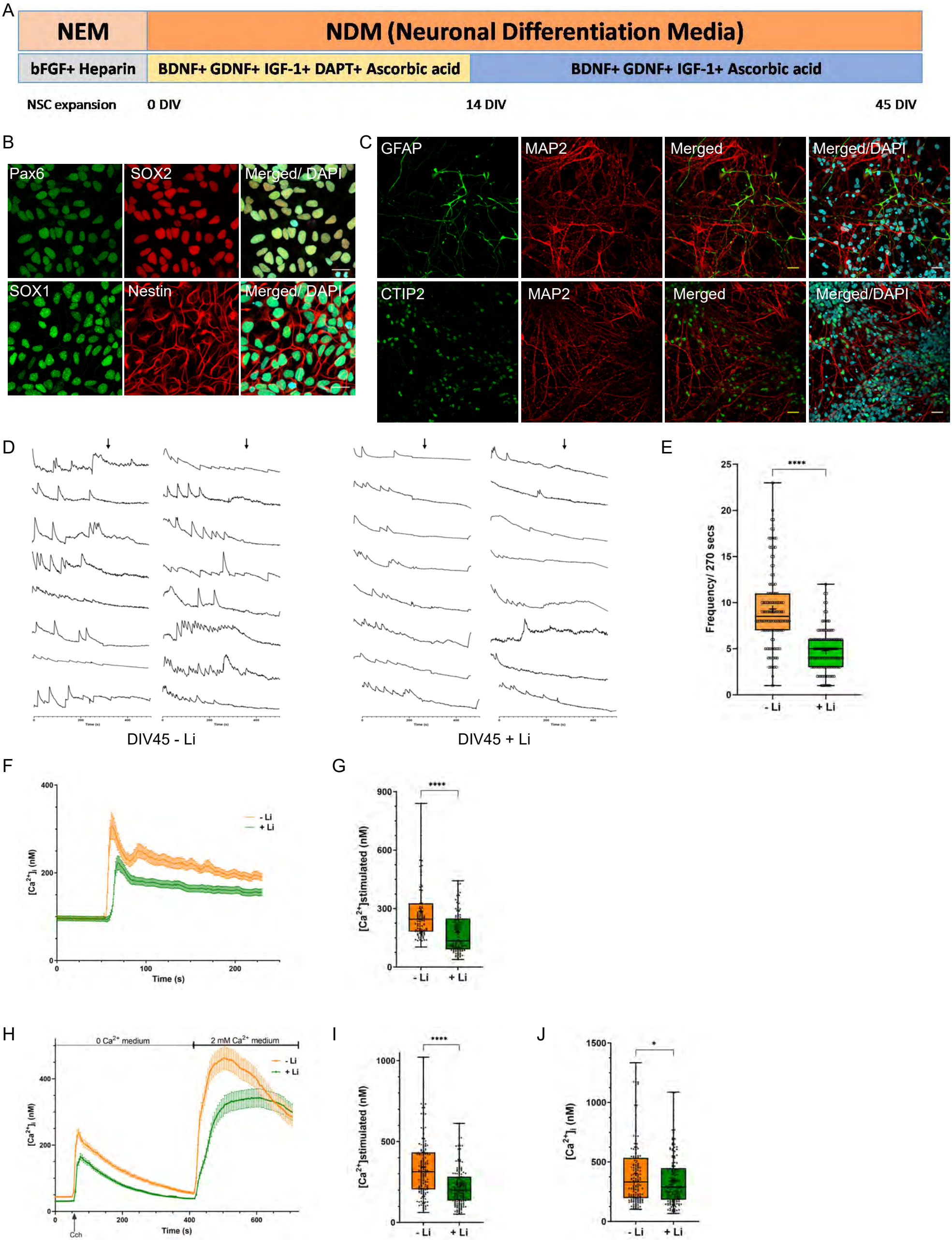

Saha Figure 4

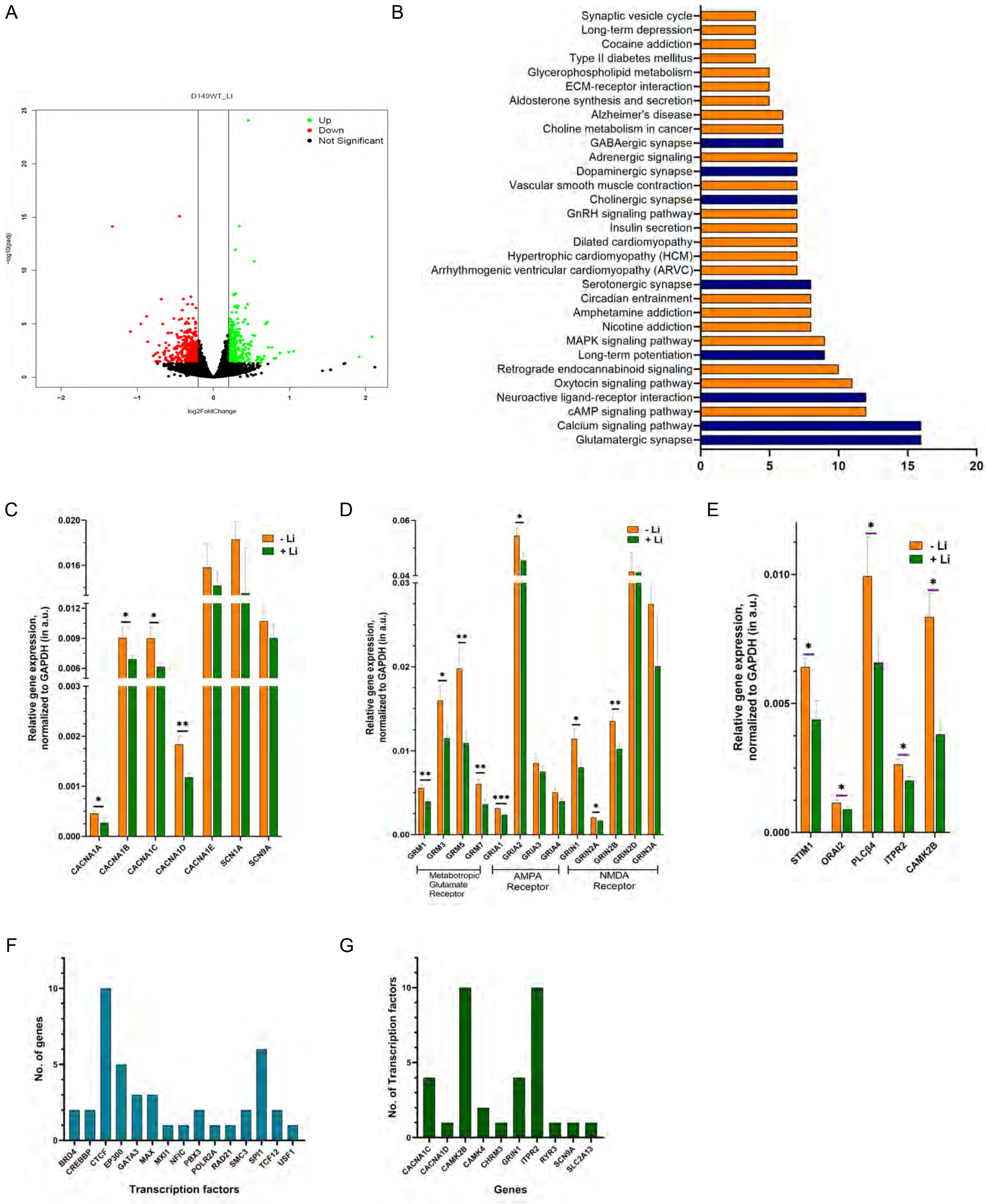

Saha Figure 5

A

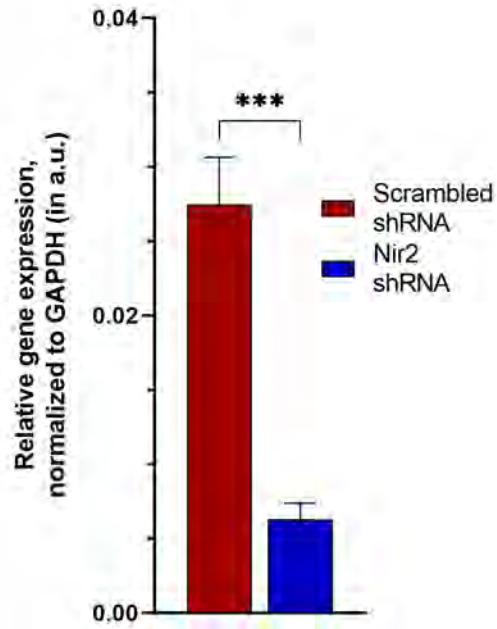

B

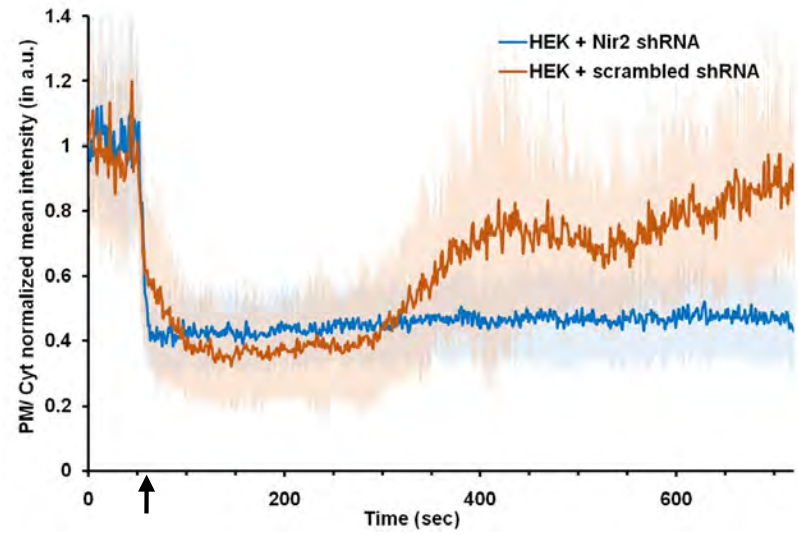

C

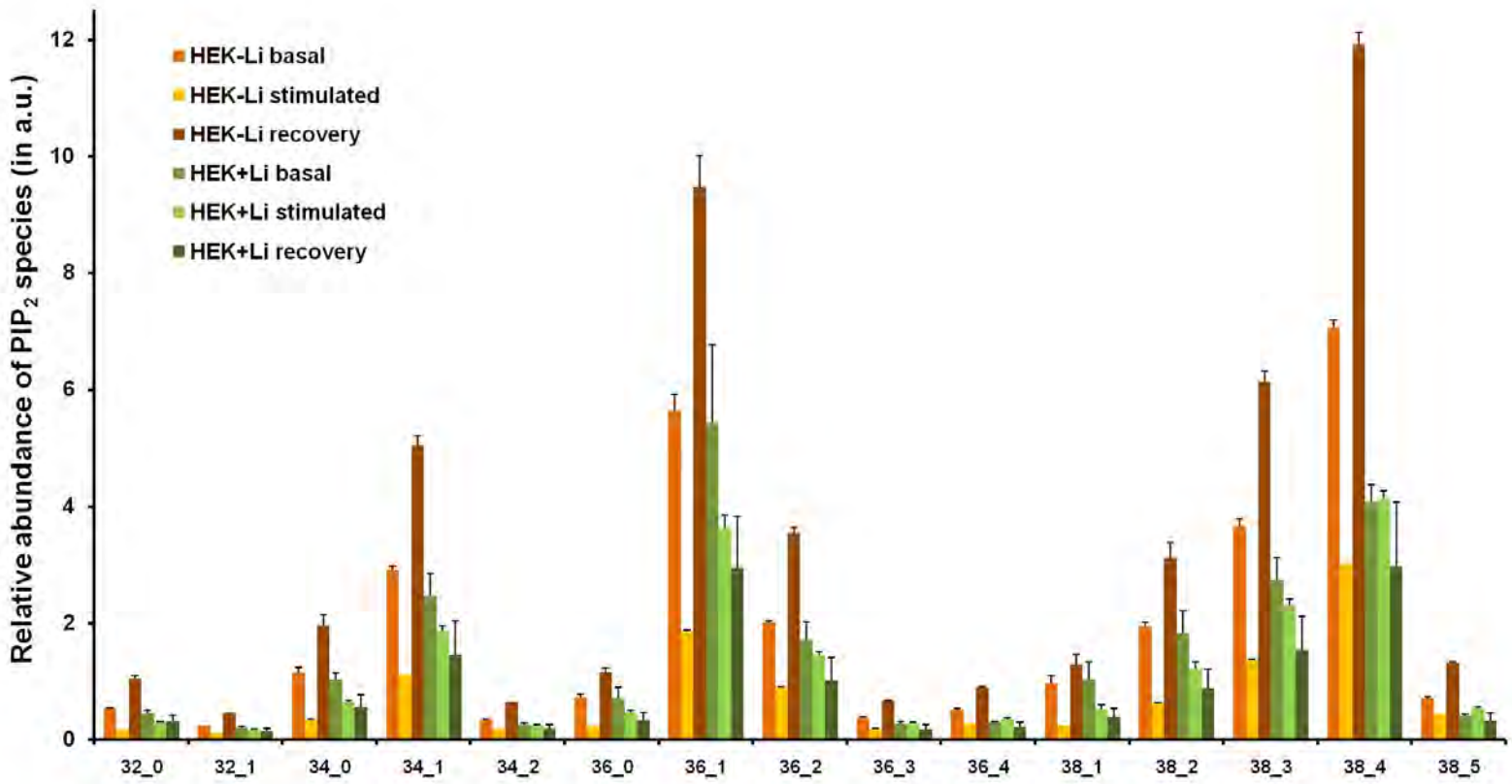

D

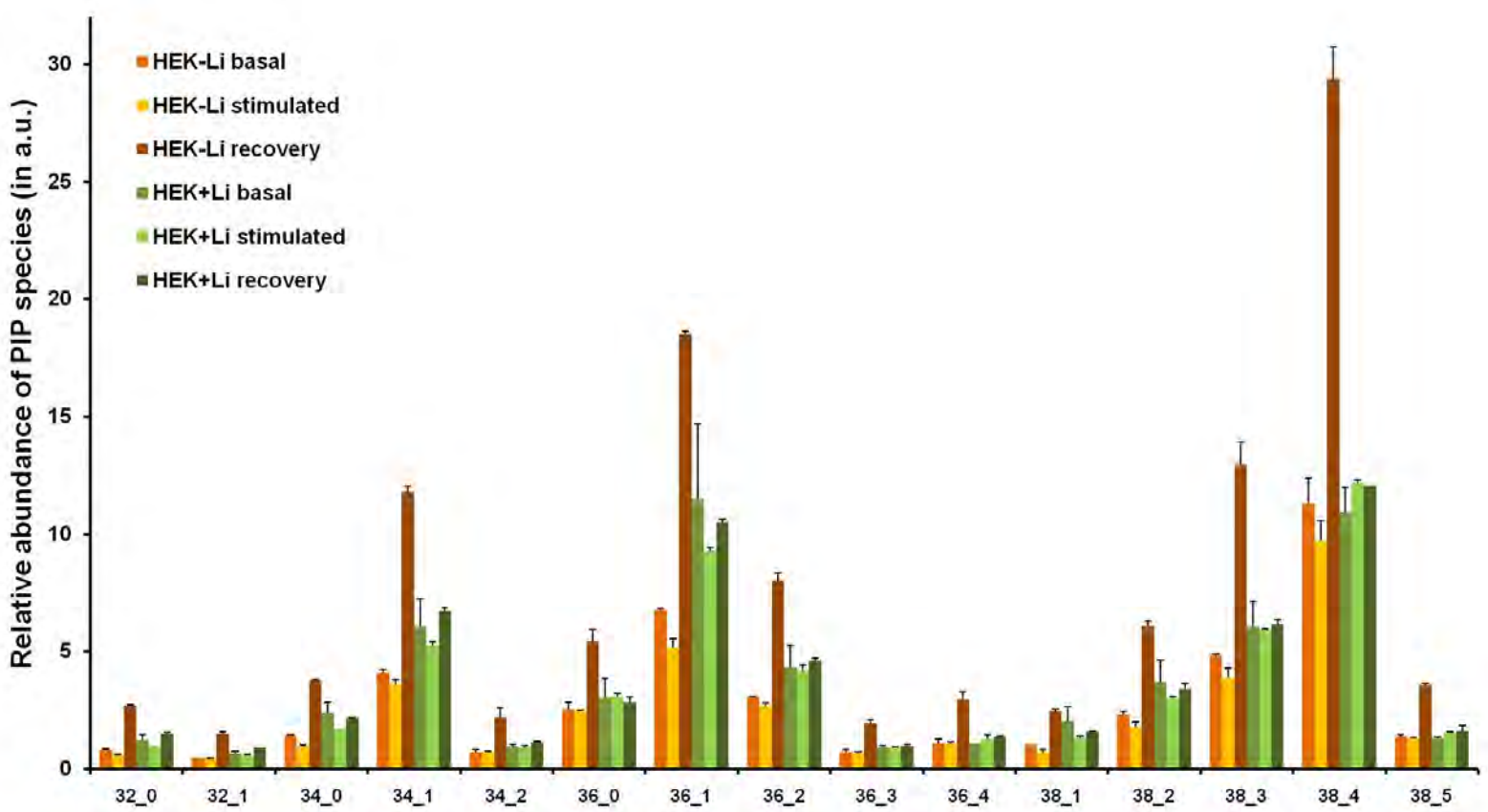

Saha Supp Figure 1

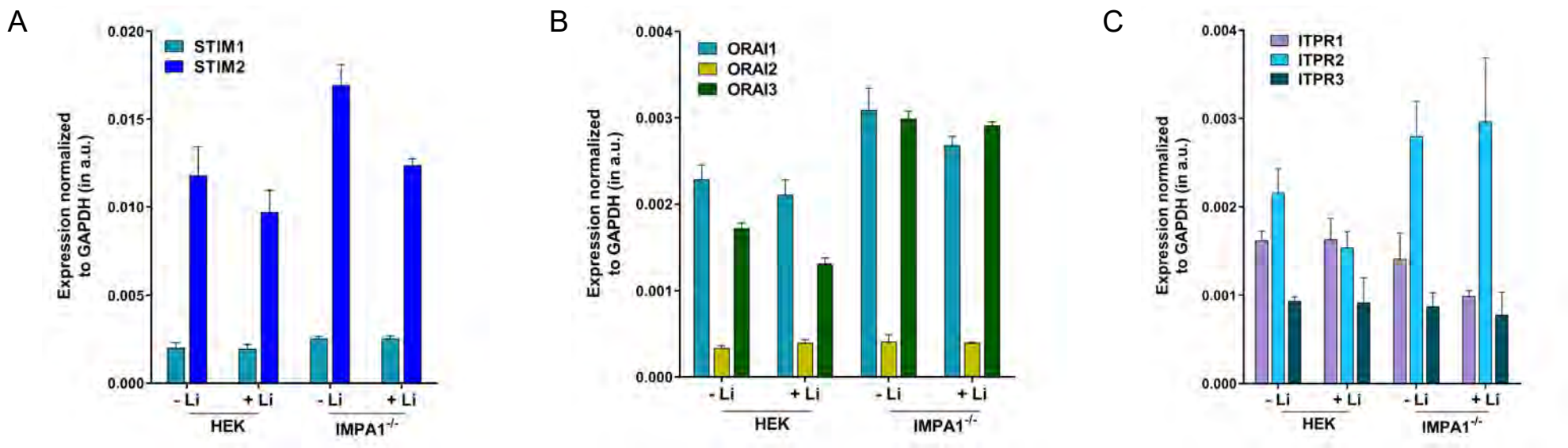

Saha Supp Figure 2

A

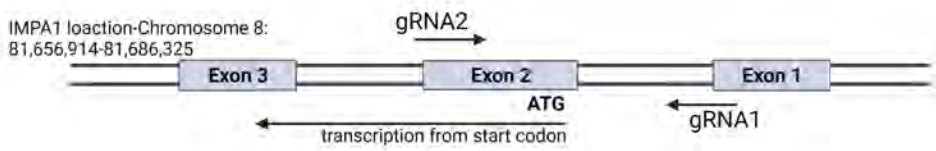

B

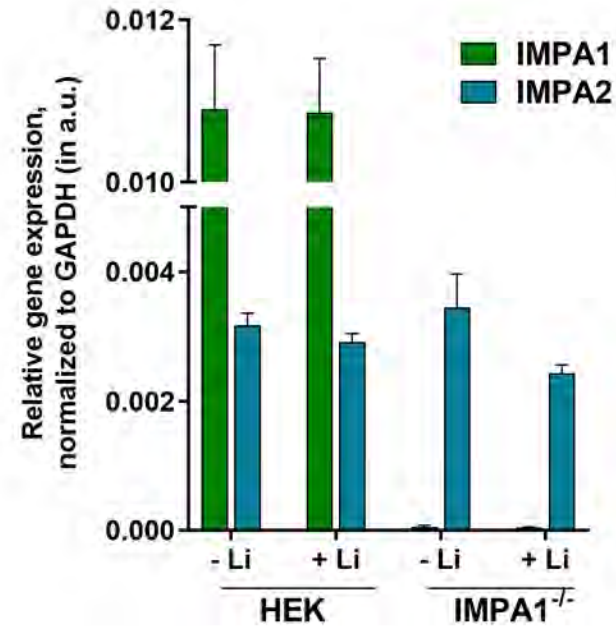

C

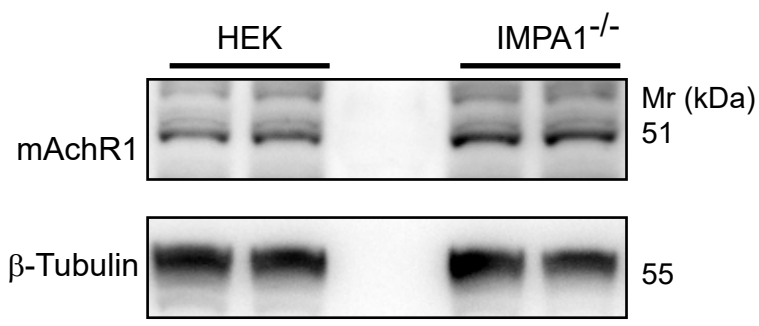

D

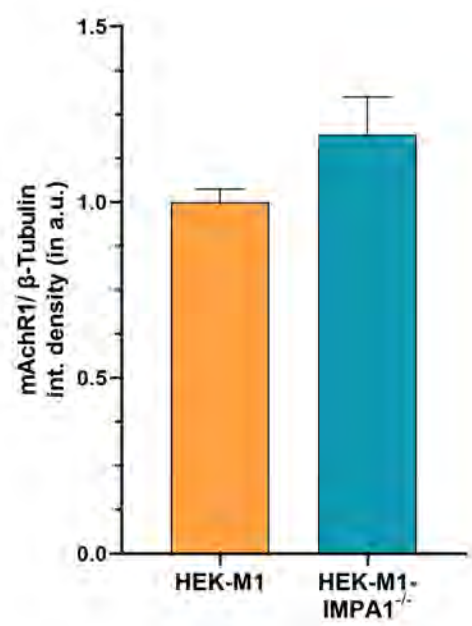

Saha Supp Figure 3

A

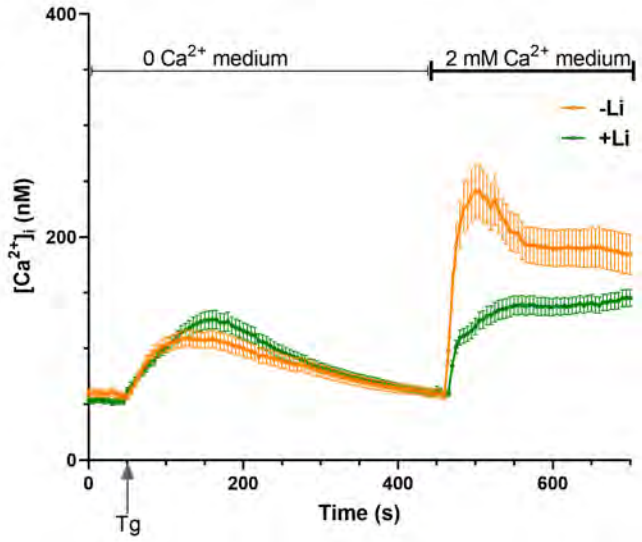

B

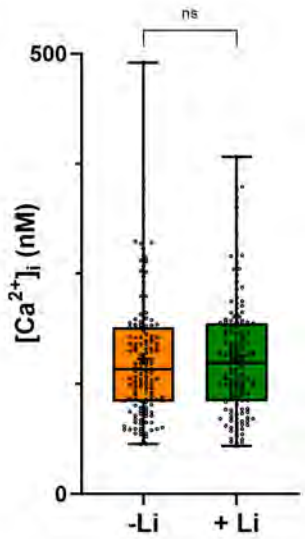

C

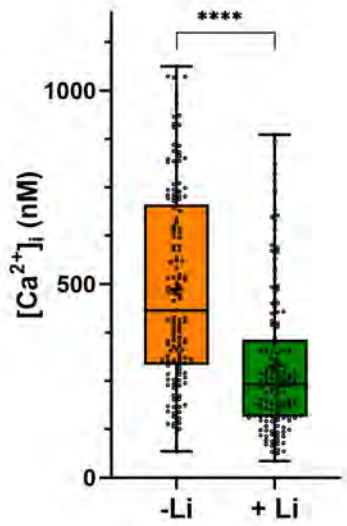

D

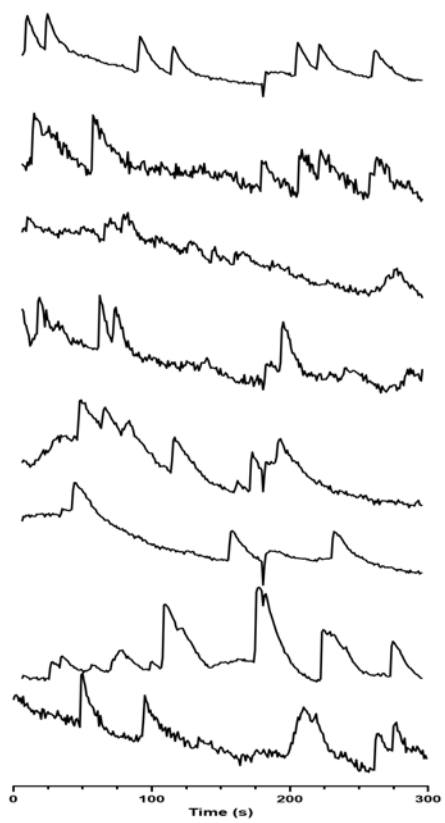

DIV30 - Li

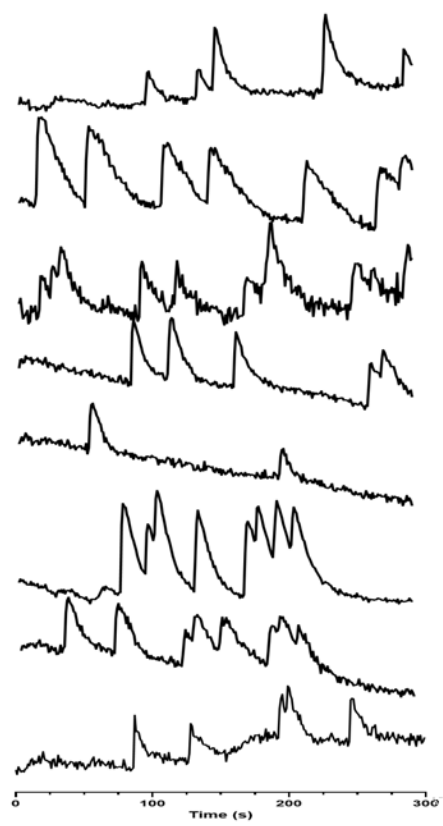

DIV30 + Li (acute)

E

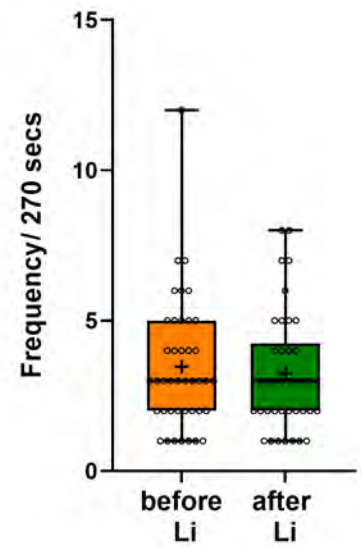

F

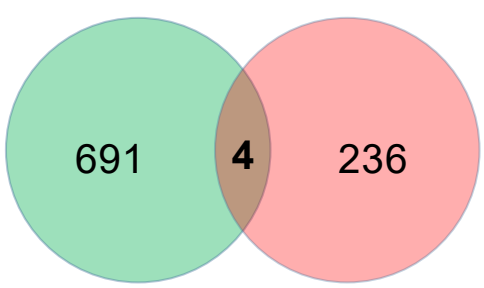

G

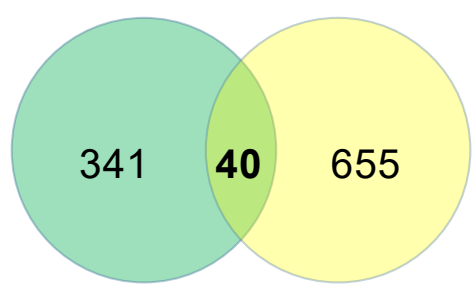

Saha Supp Figure 4

A

Gene ID	Gene name	base Mean	log2 FoldChange	pvalue	padj
ENSG00000110092	cyclinD1	1317.99	0.28	0.00	0.00
ENSG00000078018	MAP2	48889.94	-0.14	0.00	0.01
ENSG00000177606	c-Jun	4851.97	0.15	0.00	0.02
ENSG00000141510	P53	571.73	0.24	0.00	0.05
ENSG00000080815	Presenilin1	1901.77	0.15	0.01	0.09
ENSG00000103197	TSC2	2096.37	-0.15	0.01	0.10
ENSG00000070018	LRP6	4202.20	0.14	0.01	0.11
ENSG00000198561	δ-catenin	8187.44	0.09	0.02	0.13
ENSG00000134982	APC	7104.11	-0.10	0.04	0.20
ENSG00000082701	GSK3B	0.00	0.08	0.04	0.22
ENSG00000149294	NCAM	32954.36	-0.06	0.08	0.30
ENSG00000178403	Neurogenin2	286.20	0.20	0.15	0.44
ENSG00000162992	NeuroD	722.22	0.11	0.17	0.46
ENSG00000142192	APP	37645.74	0.04	0.19	0.49
ENSG00000197971	Myelin basic protein	386.66	-0.12	0.23	0.55
ENSG00000118513	c-Myb	132.05	-0.16	0.33	0.64
ENSG00000168036	β-catenin	11020.97	-0.03	0.37	0.68
ENSG00000171862	PTEN	4465.42	-0.04	0.37	0.68
ENSG00000118260	CREB	2453.46	0.05	0.40	0.71
ENSG00000161202	Dvl	3265.50	0.03	0.42	0.72
ENSG00000186868	Tau	27952.23	-0.03	0.45	0.74
ENSG00000103126	Axin	958.57	0.05	0.50	0.77
ENSG00000170365	SMAD1	738.14	0.05	0.51	0.78
ENSG00000111361	eIF2B	1238.25	0.03	0.68	0.88
ENSG00000092964	CRMP2	31852.85	-0.01	0.78	0.92
ENSG00000074054	CLASP1	6068.76	-0.01	0.83	0.94
ENSG00000131196	NFAT	68.44	-0.04	0.87	0.96
ENSG00000131711	MAP1B	98292.60	0.01	0.87	0.96
ENSG00000162946	DISC1	117.71	-0.03	0.87	0.96
ENSG00000164885	CDK5	445.92	-0.01	0.88	0.96
ENSG00000130294	Kinesin	29314.79	0.00	0.94	0.98
ENSG00000136997	c-Myc	437.65	0.00	0.98	1.00

B

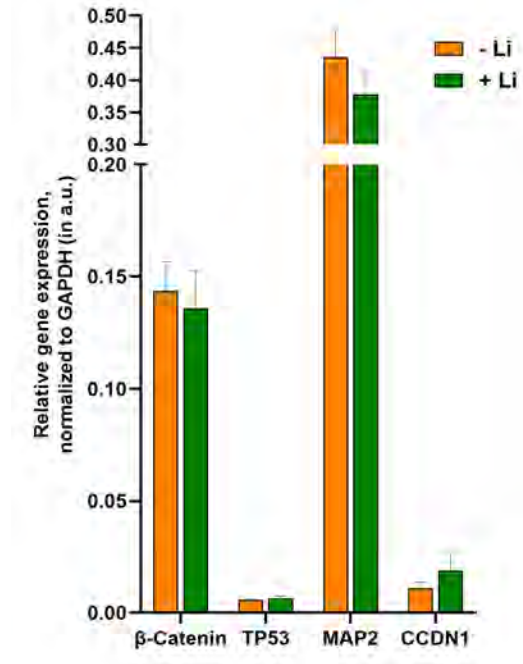

C

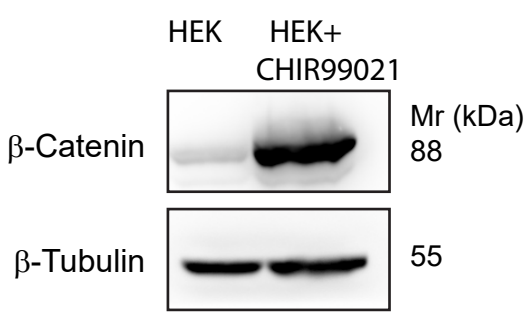

D

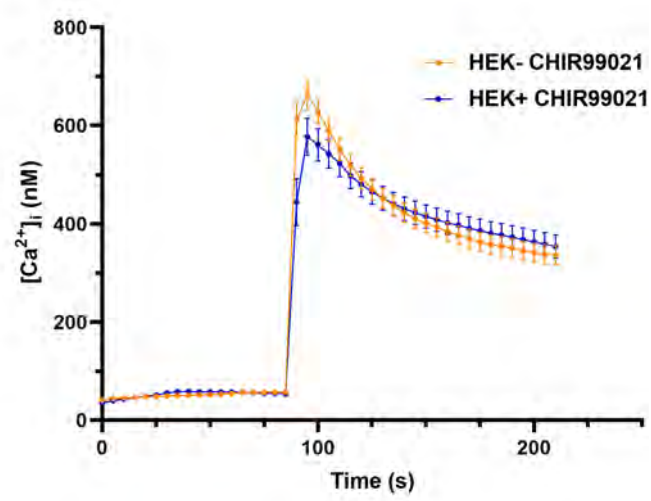

E

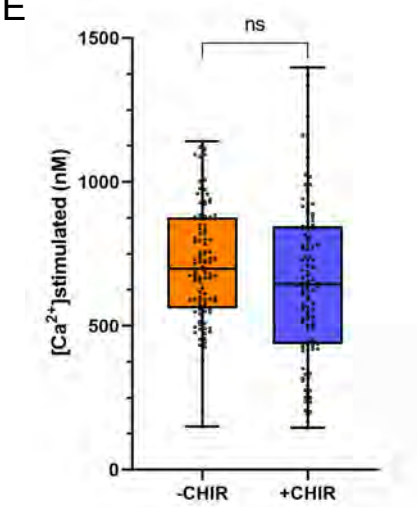

F

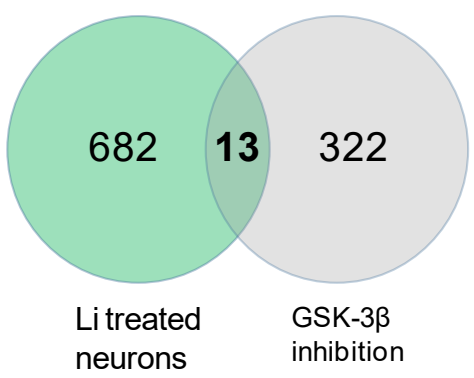

Saha Supp Figure 5